NACA TN 2913

NATIONAL ADVISORY COMMITTEE FOR AERONAUTICS

TECHNICAL NOTE 2913

ON THE DEVELOPMENT OF TURBULENT WAKES FROM VORTEX STREETS

By Anatol Roshko

California Institute of Technology

Washington
March 1953

NATIONAL ADVISORY COMMITTEE FOR AERONAUTICS

TECHNICAL NOTE 2913

ON THE DEVELOPMENT OF TURBULENT WAKES FROM VORTEX STREETS

By Anatol Roshko

SUMMARY

Wake development behind circular cylinders at Reynolds numbers from 40 to 10,000 was investigated in a low-speed wind tunnel. Standard hot-wire techniques were used to study the velocity fluctuations.

The Reynolds number range of periodic vortex shedding is divided into two distinct subranges. At $R = 40$ to 150, called the stable range, regular vortex streets are formed and no turbulent motion is developed. The range $R = 150$ to 300 is a transition range to a regime called the irregular range, in which turbulent velocity fluctuations accompany the periodic formation of vortices. The turbulence is initiated by laminar-turbulent transition in the free layers which spring from the separation points on the cylinder. This transition first occurs in the range $R = 150$ to 300.

Spectrum and statistical measurements were made to study the velocity fluctuations. In the stable range the vortices decay by viscous diffusion. In the irregular range the diffusion is turbulent and the wake becomes fully turbulent in 40 to 50 diameters downstream.

It was found that in the stable range the vortex street has a periodic spanwise structure.

The dependence of shedding frequency on velocity was successfully used to measure flow velocity.

Measurements in the wake of a ring showed that an annular vortex street is developed.

INTRODUCTION

It is always difficult to determine precisely the date and author of a discovery or idea. This seems to be the case with the periodic phenomena associated with flow about a cylinder. Although the effect

of wind in producing vibrations in wires (aeolian tones) had been known for some time, the first experimental observations are due to Strouhal (reference 1) who showed that the frequency depends on the relative air velocity and not the elastic properties of the wires. Soon after, Rayleigh (1879, references 2 and 3) performed similar experiments. His formulation of the Reynolds number dependence demonstrates his remarkable insight into the problem.

These earliest observations were concerned with the relations between vibration frequency and wind velocity. The periodic nature of the wake was discovered later, although Leonardo da Vinci in the fifteenth century had already drawn some rather accurate sketches of the vortex formation in the flow behind bluff bodies (reference 4). However, Leonardo's drawings show a symmetric row of vortices in the wake. The first modern pictures showing the alternating arrangement of vortices in the wake were published by Ahlborn in 1902 (reference 5); his visualization techniques have been used extensively since then. The importance of this phenomenon, now known as the Kármán vortex street, was pointed out by Benard (1908, reference 6).

In 1911 Kármán gave his famous theory of the vortex street (reference 7), stimulating a widespread and lasting series of investigations of the subject. For the most part these concerned themselves with experimental comparisons of real vortex streets with Kármán's idealized model, calculations on the effects of various disturbances and configurations, and so on. It can hardly be said that any fundamental advance in the problem has been made since Kármán's stability papers, in which he also clearly outlined the nature of the phenomenon and the unsolved problems. Outstanding perhaps is the problem of the periodic vortex-shedding mechanism, for which there is yet no suitable theoretical treatment.

However, the results of the many vortex-street studies, especially the experimental ones, are very useful for further progress in the problem. Attention should be drawn to the work of Fage and his associates (1927, references 8 to 10), whose experimental investigations were conducted at Reynolds numbers well above the ranges examined by most other investigators. Their measurements in the wake close behind a cylinder provide much useful information about the nature of the shedding. More recently Kovasznay (1949, reference 11) has conducted a hot-wire investigation of the stable vortex street (low Reynolds numbers), to which frequent reference will be made.

Vortex-street patterns which are stable and well-defined for long distances downstream actually occur in only a small range of cylinder Reynolds numbers, from about $R = 40$ to 150, and it is to this range that most of the attention has been given. On the other hand, as is well-known, periodic vortex shedding also occurs at higher Reynolds

numbers, up to 10^5 or more, but the free vortices which move downstream are quickly obliterated, by turbulent diffusion, and a turbulent wake is established.

The present interest in the vortex street is due to some questions arising from the study of turbulent flow behind cylinders and grids. Such studies are usually made at Reynolds numbers for which periodic vortex shedding from the cylinders or grid rods might occur. However, the measurements are always taken downstream far enough to insure that the periodic velocity fluctuations are obliterated and the flow is completely turbulent. There are several important consequences of this limitation.

First, the energy of the velocity fluctuations is quite low compared with the energy near the cylinder, and especially low compared with the dissipation represented by the form drag. In attaining the developed downstream state there is evidently not only a rapid redistribution of energy among the spectral components but also a large dissipation. Second, the theories which describe these downstream stages do not relate the flow to the initial conditions except very loosely in terms of dimensionless parameters, and it is usually necessary to determine an origin empirically (e.g., mixing-length theory or similarity theories).

On the other hand, there is evidence that some features are permanent, so that they must be determined near the beginning of the motion. One such feature is the low-wave-number end of the spectrum which (in the theory of homogeneous turbulence) is invariant.

Another is the random element. It has been pointed out by Dryden (references 12 and 13) that in the early stages of the decay of isotropic turbulence behind grids the bulk of the turbulent energy lies in a spectral range which is well approximated by the simple function $\frac{A}{1 + B^2n^2}$, characteristic of certain random processes. Liepmann (reference 14) has suggested that such a random process may be found in the shedding of vortices from the grids.

In short, there has been no description, other than very qualitative, of the downstream development of wakes which, over a wide range of Reynolds number, exhibit a definite periodicity at the beginning. The measurements reported here were undertaken to help bridge this gap.

The main results show the downstream development of the wake, in terms of energy, spectrum, and statistical properties. This development is quite different in two Reynolds number ranges, the lower one extending from about 40 to 150 and the upper, from 300 to 10^4 (and probably 10^5), with a transition range between. The lower range is the

region of the classic vortex street, stable and regular for a long distance downstream. The fluctuating energy of the flow has a discrete spectrum and simply decays downstream without transfer of energy to other frequencies. Irregular fluctuations are not developed. In the upper range there is still a predominant (shedding) frequency in the velocity fluctuations near the cylinder, and most of the energy is concentrated at this frequency; however, some irregularity is already developed, and this corresponds to a continuous spectral distribution of some of the energy. Downstream, the discrete energy, at the shedding frequency, is quickly dissipated or transferred to other frequencies, so that by 50 diameters the wake is completely turbulent, and the energy spectrum of the velocity fluctuations approaches that of isotropic turbulence.

All other features of the periodic shedding and wake phenomena may be classified as belonging to one or the other of the two ranges. This viewpoint allows some systematization in the study of wake development.

In particular, it is felt that the possibilities of the vortex street are by no means exhausted. A study of the interaction of periodic fluctuations with a turbulent field seems to be a fruitful approach to the turbulence problem itself. It is planned to continue the present work along these lines.

From a more immediately practical viewpoint an understanding of the flow close to a bluff cylinder is important in at least two problems, namely, structural vibrations in members which themselves shed vortices and structural buffeting experienced by members placed in the wakes of bluff bodies. Many of these are most appropriately treated by the statistical methods developed in the theories of turbulence and other random processes (reference 15). These methods are easily extended to include the mixed turbulent-periodic phenomena associated with problems such as the two mentioned above.

The research was conducted at GALCIT under the sponsorship and with the financial assistance of the National Advisory Committee for Aeronautics, as part of a long-range turbulence study directed by Dr. H. W. Liepmann. His advice and interest throughout the investigation, as well as helpful discussions with Dr. Paco Lagerstrom, are gratefully acknowledged.

SYMBOLS

A,B	constants
a,b	major and minor axis, respectively, of correlation ellipse

C_D	drag coefficient
C_{D_P}	form drag coefficient
$C = \sqrt{N_2}/N_1$	
D	outside diameter of ring
d	cylinder dimension
d'	distance between free vortex layers
d_s	diameter of ring-supporting wire
E	wake energy
E_1, E_2	components of wake energy due to periodic fluctuations
F	dimensionless frequency $\left(\frac{n_1 d^2}{\nu}\right)$
F(n)	energy spectrum
$F_1(n), F_2(n)$	energy spectra of discrete energy
$F_r(n)$	continuous energy spectrum
$G(n_A)$	output of wave analyzer at setting n_A
h	lateral spacing of vortices
h'	initial lateral spacing of vortices
h*	lateral spacing between positions of u'_m
K	constant
k	integer
L	scale
L_z	scale corresponding to R_z
l	downstream spacing of vortices
M_k	moment, of order k, of probability density

N_k	"absolute" moment of probability density
n_1	shedding frequency
$n_2 = 2n_1$	
$P(\xi)$	probability distribution function
$p(\xi)$	probability density
Q	area under response characteristic
$q(r)$	tangential velocity in vortex
$q^* = q(r^*)$	
R	Reynolds number
$R(n)$	response characteristic of wave analyzer
R_D	Reynolds number based on ring diameter
$R_t(\tau)$	time correlation function
$R_z(\zeta)$	space correlation function
r	distance from vortex center
r^*	radius of vortex
S	Strouhal number, based on cylinder dimension $\left(n_1 d/U_o\right)$
S'	Strouhal number, based on distance between free vortex layers $\left(n_1 d'/U_o\right)$
T	time scale
T_a	time of averaging
t	time
U	local mean velocity in x-direction
U_o	mean stream velocity
U^*	mean velocity at vortex center

u,v,w	components of velocity fluctuation
u_1,u_2	periodic velocity fluctuations, at frequencies n_1 and n_2
u_r	random velocity fluctuation
u'_m	peak root-mean-square value of velocity fluctuation
V	velocity of vortex relative to the fluid
x,y,z	reference axes and distance from center of cylinder
α	flatness factor of probability distribution $\left(M_4/M_2^2\right)$
Γ	strength (circulation) of a vortex
$\delta(n)$	Dirac delta function
ϵ	positive number
ζ	distance between two points, measured in z-direction
η	dimensionless frequency $\left(\frac{L}{U_o} n\right)$
θ	dimensionless "time" in life of vortex $\left(\frac{U_o}{U^*} \frac{x}{d}\right)$
μ	dummy variable
ν	kinematic viscosity
ξ	a value of u
ρ	density
σ	skewness of probability distribution $\left(M_3/M_2^{3/2}\right)$
τ	time interval
φ	dimensionless spectrum $\left(\frac{U_o F_r(n)}{L}\right)$
ω	half band width of wave analyzer

GENERAL CONSIDERATIONS

Except for the parameters directly related to the shedding frequency, the quantities measured were essentially those that are standard in turbulence investigations (cf. references 12 to 14). These are briefly reviewed below with some modifications required to study the periodic features.

Reference Axes

The origin of axes is taken at the center of the cylinder (fig. 1); x is measured downstream in the direction of the free-stream velocity, z is measured along the axis of the cylinder, which is perpendicular to the free-stream velocity, and y is measured in the direction perpendicular to (x,y); that is, $y = 0$ is the center plane of the wake. The free-stream velocity is U_o and the local mean velocity in the x-direction is U. The fluctuating velocities in the x, y, and z directions are u, v, and w, respectively. The flow is considered to be two-dimensional; that is, mean values are the same in all planes z = Constant.

Shedding Frequency

The shedding[1] frequency is usually expressed in terms of the dimensionless Strouhal number $S = n_1 d/U_o$, where n_1 is the shedding frequency (from one side of the cylinder), d is the cylinder diameter, and U_o is the free-stream velocity. The Strouhal number S may depend on Reynolds number, geometry, free-stream turbulence level, cylinder roughness, and so forth. The principal geometrical parameter is the cylinder shape (for other than circular cylinders, d is an appropriate dimension). However, cylinder-tunnel configurations must be taken into account, for example, blockage and end effects. In water-channel experiments surface effects may have an influence. Usually the geometrical configuration is fixed, and then S is presented as a function of Reynolds number R.

Instead of Strouhal number it is sometimes convenient to use the dimensionless parameter $F = n_1 d^2/\nu$, where ν is the kinematic viscosity.

---

[1]The term "shedding" is used throughout this report, for convenience; it is not meant to imply anything about the mechanism of the formation of free vortices.

Energy

The experiments to be described are concerned mainly with the velocity fluctuation in the wake, and especially with the corresponding energy.

The energy of the velocity fluctuation at a point in the fluid is $\frac{1}{2}\rho(u^2 + v^2 + w^2)$ per unit volume, where (u,v,w) is the fluctuating velocity and the bar denotes an averaging (see the section "Distribution Functions"). In these experiments only the component u was measured, and the term "energy" is used to denote the energy in that component only.

The energy intensity is defined as $\overline{(u/U_o)^2}$. Since the mean flow is two-dimensional the intensity does not vary in the z-direction. At any downstream position in the wake it varies in the y-direction, normal to the wake. The integral of the intensity over a plane normal to the free stream (per unit span) is called the wake energy E:

$$E = \int_{-\infty}^{\infty} \overline{\left(\frac{u}{U_o}\right)^2} d\left(\frac{y}{d}\right) \tag{1}$$

The velocity fluctuation in the wake of a shedding cylinder displays a predominant frequency (as well as harmonics) which is the shedding frequency. However, except in a small Reynolds number range, the fluctuation has random irregularities "superimposed" on it; that is, it is not purely periodic, in the mathematical sense. However, it is convenient to speak of the "periodic" and "random" or turbulent parts of the fluctuation.[2] The energy may be written

$$\overline{u^2} = \overline{u_r^2} + \overline{u_1^2} + \overline{u_2^2} \tag{2}$$

where $\overline{u_r^2}$ is that portion of the energy contributed by the random (turbulent) fluctuation, $\overline{u_1^2}$ is contributed by the periodic fluctuation at the shedding frequency n_1, and $\overline{u_2^2}$ corresponds to twice the shedding frequency $n_2 = 2n_1$. (The center of the wake feels the

[2] A turbulent fluctuation is an irregular variation, with respect to time, which is characterized in particular by its randomness and absence of periodicity (cf. reference 13, p. 9).

influence of vortices from both sides and n_2 is prominent there, at least near the "beginning" of the wake. Higher harmonics are found to be negligible.)

Equation (2) is a kind of spectral resolution, in which $\overline{u_1^2}$ and $\overline{u_2^2}$ are the energies at the specific frequencies n_1 and n_2. This type of resolution is called a discrete, or line, spectrum. But $\overline{u_r^2}$ is not a discrete spectral component for it is the energy in the turbulent part of the fluctuation and contains "all" frequencies. It has a continuous frequency distribution of energy, for which a slightly different definition of spectrum is appropriate. This is postponed until the following section.

Corresponding to equation (2), an equation may be written for the wake energy E and its turbulent and periodic components:

$$E = E_r + E_1 + E_2 \tag{3}$$

Of particular interest will be the fraction of discrete energy $(E_1 + E_2)/E$ at various stages of wake development.

Correlation Functions; Spectrum

Definitions.- The time correlation function of the fluctuation $u(t)$ is defined by

$$R_t(\tau) = \frac{\overline{u(t)u(t + \tau)}}{\overline{u^2}} \tag{4}$$

where τ is a time interval. The time scale is then defined by

$$T = \int_0^\infty R_t \, d\tau \tag{5}$$

The Fourier transform of R_t defines another function

$$F(n) = 4 \int_0^\infty R_t(\tau) \cos 2\pi n\tau \, d\tau \tag{6}$$

Then, also

$$R_t(\tau) = \int_0^\infty F(n) \cos 2\pi n\tau \, d\tau \tag{7}$$

For $\tau = 0$, equations (4) and (7) give

$$R_t(0) = \int_0^\infty F(n) \, dn = 1 \tag{8}$$

where $F(n)$ is defined as the energy spectrum; that is, $F(n)\,dn$ is the fraction of the energy in the frequency interval n to $n + dn$. It is the fraction of energy "per unit frequency," as contrasted with the discrete energy spectrum discussed in the section "Energy."

In studies of isotropic turbulence, at Reynolds numbers corresponding to those in the present experiments, it is found that the energy spectrum is well represented by the form

$$F(n) = \frac{A}{1 + B^2n^2} \tag{9}$$

or, what amounts to the same thing, that the correlation function is of the form

$$R_t(\tau) = e^{-K\tau} \tag{10}$$

If the normalizing factor $K = U_o/L$ is used in equation (10), L being a characteristic length, then equation (6) gives

$$\frac{U_oF(n)}{L} = \frac{4}{1 + 4\pi^2\left(L^2n^2/U_o^2\right)} \tag{11a}$$

which may be conveniently written in terms of the dimensionless parameters

$$\varphi = U_oF(n)/L \tag{12a}$$

and

$$\eta = \frac{L}{U_o} n \tag{12b}$$

Then

$$\varphi = \frac{4}{1 + (2\pi\eta)^2} \tag{11b}$$

It is clear from equations (5) and (10) that L is a length scale related to the time scale by

$$L = U_o T \tag{13}$$

Equation (11b) is used as a convenient reference curve to compare the measurements reported below.

Periodic functions.- The energy spectrum $F(n)$ is particularly well suited to turbulent fluctuations, for which the energy is continuously distributed over the frequencies. For periodic fluctuations the discrete, or line, spectrum is more appropriate, but in the present "mixed" case it is convenient to write the discrete energy, also, in terms of $F(n)$. This may be done by using the Dirac delta function $\delta(n)$. Thus the energy at the shedding frequency n_1 is

$$\overline{u_1^2} = \overline{u_1^2} \int_0^\infty \delta(n - n_1)\, dn \tag{14}$$

that is,

$$F_1(n) = \delta(n - n_1) \tag{15}$$

Then the mixed turbulent-periodic fluctuations in the wake of a shedding cylinder are considered to have an energy spectrum which is made up of continuous and discrete parts (cf. equation (2) and appendix A):

$$\overline{u^2} \int_0^\infty F(n)\, dn = \overline{u_r^2} \int_0^\infty F_r(n)\, dn + \overline{u_1^2} \int_0^\infty F_1(n)\, dn + \overline{u_2^2} \int_0^\infty F_2(n)\, dn \tag{16}$$

that is,

$$F(n) = \frac{\overline{u_r^2}}{\overline{u^2}} F_r(n) + \frac{\overline{u_1^2}}{\overline{u^2}} \delta(n - n_1) + \frac{\overline{u_2^2}}{\overline{u^2}} \delta(n - n_2) \tag{17}$$

Space correlation function; phase relations.- The correlation function defined in equation (4) describes the time correlation. Another correlation function which is useful in the present study is one which relates the velocity fluctuations at two points in the wake, situated on a line parallel to the cylinder. This is defined by

$$R_z(\zeta) = \frac{\overline{u(z,t)u(z + \zeta,t)}}{\overline{u^2}} \tag{18}$$

where ζ is the distance between the two points. The corresponding scale is

$$L_z = \int_0^\infty R_z \, d\zeta \tag{19}$$

The function R_z should be particularly suited to studying turbulent development. Close to the cylinder it should reflect the regularity connected with the periodic shedding, especially in a regular, stable vortex street, in which there are no turbulent fluctuations. When there are turbulent fluctuations and, especially, far downstream where there is no more evidence of periodicity, R_z should be typical of a turbulent fluid; that is, the correlation should be small for large values of ζ.

The function R_z may be obtained by standard techniques applied to the two signals $u(z,t)$ and $u(z + \zeta,t)$. One well-known visual method is to apply the signals to the vertical and horizontal plates, respectively, of an oscilloscope and to observe the resulting "correlation figures" (or ellipses) on the screen (reference 16). If the signals $u(t)$ are turbulent fluctuations then the light spot moves irregularly on the screen, forming a light patch which is elliptic in shape. The correlation function is given by

$$R_z = \frac{a^2 - b^2}{a^2 + b^2} \tag{20}$$

where a and b are the major and minor axes of the ellipse.

If $u(z,t)$ is a periodic function, in both time and space, then the correlation figure is an elliptical loop (Lissajous figure) whose major and minor axes again give R_z according to equation (20). Such a case would exist if the wake had a spanwise periodic structure. Then $R_z(\zeta)$ would be periodic. A special case of this is $R_z(\zeta) = 1$, as would be expected in a vortex street, provided the vortex filaments are straight and parallel to the cylinder and do not "wobble."

Distribution Functions

Random functions.- The probability density $p(\xi)$ of a randum function $u_r(t)$ is defined as the probability of finding u_r in the interval $(\xi,\xi + d\xi)$. It may be found by taking the average of observations made on a large number (ensemble) of samples of $u_r(t)$, all these observations being made at the same time t. This is called an ensemble average. If $u_r(t)$ is a stationary process, as in the present case, then appeal is made to the ergodic hypothesis and the ensemble average is replaced by the time average, obtained by making a large number of observations on a single sample of $u_r(t)$. The probability density $p(\xi)$ is the number of times that u_r is found in $(\xi,\xi + d\xi)$ divided by the total number of observations made. In practice, time averages are more convenient than ensemble averages. The averaging time T_a must be large enough so that a statistically significant number of observations are made. This imposes no hardship; it is sufficient that T_a be large compared with the time scale T. If necessary, the error can be computed.

Experimentally, $p(\xi)$ may be determined by the principle illustrated below:

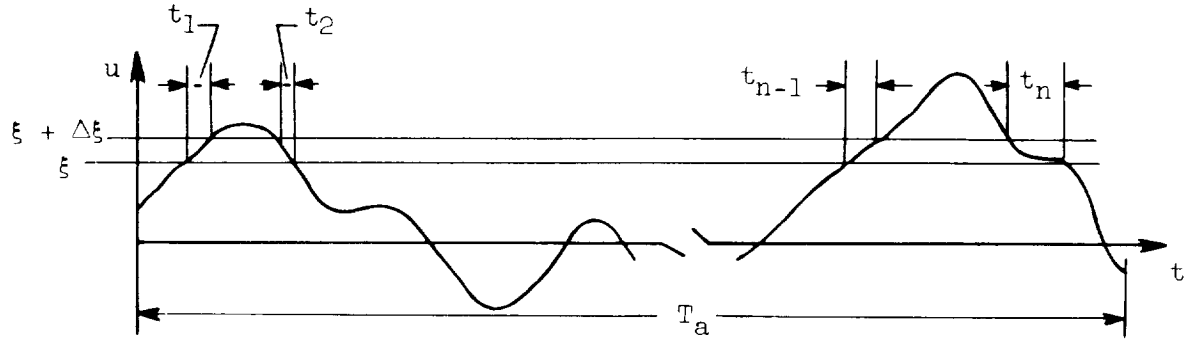

$$p(\xi) \approx \frac{\sum_{1}^{n} t_i}{T_a} \tag{21}$$

$$t_i = \frac{\Delta\xi}{|du_r/dt|} \tag{22}$$

The most elementary application of this principle is a graphical one using a photographic trace of $u_r(t)$. More conveniently, electronic counting apparatus is employed (see the section "Statistical Analyzer").

The statistics of $u_r(t)$ are usually described in terms of the moments of $p(\xi)$ and certain functions derived from the moments. The

moment of order k is defined as

$$M_k = \int_{-\infty}^{\infty} \xi^k p(\xi)\, d\xi \tag{23}$$

Another useful definition is

$$N_k = \int_{-\infty}^{\infty} \left|\xi^k\right| p(\xi)\, d\xi \tag{24}$$

where N_k is equal to M_k for even values of k. If $p(\xi)$ is symmetrical, then M_k is 0 for odd values of k but N_k is not.

From the definition of $p(\xi)$ it follows that $M_0 = \int_{-\infty}^{\infty} p(\xi)\, d\xi = 1$; ξ will be normalized by requiring that $M_2 = 1/2$, that is, the mean-square value $\overline{u_r^2} = 1/2$.

Three useful functions derived from the moments are

$$C = \frac{N_2^{1/2}}{N_1} = \frac{M_2^{1/2}}{N_1} \tag{25}$$

Skewness $$\sigma = \frac{M_3}{M_2^{3/2}} \tag{26}$$

Flatness $$\alpha = \frac{M_4}{M_2^2} \tag{27}$$

Periodic functions.- The above definitions may be extended to the case of a periodic function $u_1(t)$. The probability density can be completely determined from a single wave length of $u_1(t)$; that is, it is sufficient to take T_a equal to the period. This complete a priori information is a basic difference between periodic and random functions.[3]

[3]For a periodic function the ergodic principle may not be invoked; the ensemble average and the time average are not the same (unless the members of the ensemble have random phase differences). It is the time average that is computed here, for comparison with the experimental results, which are also time averages.

If $u_1(t)$ is measured experimentally then $t_i(\xi)$ in equation (21) can also be measured. If $u_1(t)$ is given in analytic form then $t_i(\xi)$ may be calculated from equation (22). Thus the distribution densities for simple wave shapes are easily calculated. Table I gives the probability densities and moments for the triangular wave, sine wave, and square wave. Also included is the Gaussian probability density, which is a standard reference for random functions.

The moments of the probability densities of these wave shapes are shown in figure 2. The moments for the random function increase much faster than those for the periodic functions. This results from the fact that the maximum values of a periodic function are fixed by its amplitude, while for a random function all values are possible.

The probability density of a function which is partly periodic and partly random is expected to display the transition from one type to the other. The tendency toward the random probability density should be strong. For instance, random fluctuations in the amplitude of a sine wave result in a large increase in the higher moments. It is interesting to study the relation between probability functions and spectra, particularly the case where most of the energy is discrete but the fluctuation amplitude is random.

EXPERIMENTAL DATA

Wind Tunnel

The experiments were all made in the GALCIT 20- by 20-inch low-turbulence tunnel (fig. 1). The turbulence level is about 0.03 percent. The wind velocity may be varied from about 50 centimeters per second (1 mph) to 1200 centimeters per second (25 mph).

Cylinders

The cylinders used in the experiments varied in diameter from 0.0235 to 0.635 centimeter. Music wire or drill rod was used. The diameter tolerances are about 0.0002 centimeter. The cylinders spanned the tunnel so that the length in all cases was 50 centimeters (20 in.); the cylinders passed through the walls and were fastened outside the tunnel.

Rings

Some studies were made of the flow behind rings. These were made up of wire. Each ring was supported in the tunnel by three thin support wires, attached to the ring circumference at 120° intervals. Table II gives the dimensions of the rings used (where d is the wire diameter, D, the ring diameter, and d_s, the diameter of the support wire).

Velocity Measurements

Velocities higher than about 400 centimeters per second were measured with a pitot tube, calibrated against a standard. The pressures were read on a precision manometer to an accuracy of about 0.002 centimeter of alcohol. Velocities lower than 400 centimeters per second were determined from the shedding frequency of a reference cylinder (0.635 cm), as explained in the section "Use of Shedding Frequency for Velocity Measurements."

Fluctuating velocities were measured with a hot-wire anemometer (1/20 mil platinum). Only $u(t)$, the fluctuating velocity in the flow direction, has been measured so far. The hot-wire was always parallel to the cylinder.

Traversing Mechanism

The hot-wire was mounted on a micrometer head which allowed it to be traversed normal to the wake and positioned to 0.001 centimeter. The head was mounted on a horizontal lead screw which allowed traversing in the flow direction, in the center plane of the tunnel. The positioning in this direction was accurate to about 0.01 centimeter. The horizontal lead screw could be turned through 90° to allow traversing parallel to the cylinder, for correlation or phase measurements (section "Space correlation function; phase relations"). For this purpose, a second micrometer head with hot-wire could be set up in a fixed position along the line of traverse of the first hot-wire. Then correlations could be measured between this point and the movable one.

Electronic Equipment

The hot-wire output was amplified by an amplifier provided with compensation up to 10,000 cycles per second. The amplifier output could be observed on an oscilloscope screen or measured on a Hewlett-Packard Model 400c vacuum-tube voltmeter. Values of $\overline{u^2}$ were obtained by reading the root-mean-square voltage on the voltmeter. (This voltmeter is actually an average-reading meter; it reads true root-mean-square values

only for a sine wave. A few of the indicated root-mean-square values, for turbulent velocity fluctuations, were checked against true root-mean-square values as obtained from the statistical analyzer (see the section "Statistical Analyzer"); these may differ up to 10 percent, depending on the wave shape, but, at present, no corrections have been made, since the absolute values were not of prime interest.) Usually only relative values of $\overline{u^2}$ were required, but absolute values could be determined by comparing the voltage with that obtained by placing the hot-wire behind a calibrated grid.

The frequencies of periodic fluctuations were determined by observing Lissajous figures on the oscilloscope; that is, the amplifier output was placed on one set of plates and a known frequency on the other. This reference frequency was taken from a Hewlett-Packard Model 202B audio oscillator, which supplied a frequency within 2 percent of that indicated on the dial.

Frequency Analyzer

Spectra were measured on a Hewlett-Packard Model 300A harmonic wave analyzer. This analyzer has an adjustable band width from 30 to 145 cycles per second (defined in appendix A) and a frequency range from 0 to 16,000 cycles. The output was computed directly from readings of the voltmeter on the analyzer. It was not felt practicable to read output in the frequency range below 40 cycles; therefore, the continuous spectrum was extrapolated to zero frequency.

To determine the discrete spectrum in the presence of a continuous background some care was required. In such cases the analyzer reading gives the sum of the discrete spectral energy and a portion of that in the continuous spectrum, the proportions being determined by the response characteristic of the wave analyzer. The value in the continuous part was determined by interpolation between bands adjacent to the discrete band and subtracted out to give the discrete value, as outlined in more detail in appendix A.

Statistical Analyzer

The statistical analyzer, designed to obtain probability functions, operates on the principle described in the section "Distribution Functions;" here $u(t)$ is a voltage signal. A pulse train (fig. 3) is modulated by $u(t)$ and is then fed into a discriminator which "fires" only when the input pulses exceed a certain bias setting, that is, only when $u(t) > \xi$. For each such input pulse the discriminator output is a pulse of constant amplitude. The pulses from the discriminator are counted by a series of electronic decade counters terminating in a mechanical counter.

The complete analyzer consists of 10 such discriminator-counter channels, each adjusted to count above a different value of ξ. It will be seen that the probability function obtained is the integral of the probability density described in the section "Distribution Functions;" that is,

$$P(\xi) = \text{Probability that } u(t) > \xi$$

$$= \int_{\xi}^{\infty} p(\mu)\, d\mu$$

It is possible to rewrite the moments (section "Distribution Functions") in terms of $p(\xi)$, a more convenient form for calculation with this analyzer. These are also shown in table I.

More complete details of the analyzer and computation methods may be found in references 17 and 18.

RESULTS

Shedding Frequency

Since Strouhal's first measurements in 1878 (reference 1) the relation between the shedding frequency and the velocity has been of interest to many investigators. Rayleigh (reference 2, p. 413) pointed out that the parameter $n_1 d/U_0$ (now called the Strouhal number S) should be a function of the Reynolds number. Since then there have been many measurements of the relationship (reference 19, p. 570). One of the latest of these is the measurement by Kovasznay (reference 11), whose determination of $S(R)$ covers the range of R from 0 to 10^4. Kovasznay also made detailed investigations of the vortex-street flow pattern at low Reynolds numbers. He observed that the street is developed only at Reynolds numbers above 40 and that it is stable and regular only at Reynolds numbers below about 160.

The present measurements of $S(R)$ are given in figures 4 and 5. Except at Reynolds numbers between 150 and 300, the scatter is small, and the measurements agree with those of Kovasznay. The large number of cylinder sizes used results in overlapping ranges of velocity and frequency so that errors in their measurement should be "smeared" out. It is believed that the best-fit line is accurate to 1 percent.

The measurements are corrected for tunnel blockage but no attempt is made to account for end effects. With the cylinder sizes used no systematic variations were detected.

Nature of Velocity Fluctuations

It was observed, as in Kovasznay's work, that a stable, regular vortex street is obtained only in the Reynolds number range from about 40 to 150. The velocity fluctuations in this range, as detected by a hot-wire, are shown on the oscillograms in figure 6, for a Reynolds number of 80. These were taken at two downstream positions, $x/d = 6$ and 48, and at several values of y/d. (The relative amplitudes are correct at each value of x/d, but the oscillograms for $x/d = 48$ are to a larger scale than those for $x/d = 6$.) The frequencies and amplitudes are quite steady; it is quite easy to determine the frequencies from Lissajous figures (section "Electronic Equipment"), which, of course, are also steady.

Another example, at $R = 145$, is shown in figure 7(a). (The double signal was obtained for correlation studies and is referred to later in the section "Spanwise Correlation and Phase Measurements." The dotted nature of the trace is due to the method of obtaining two signals on one screen, using an electronic switch.)

At Reynolds numbers between about 150 and 300 there are irregular bursts in the signal. An example is shown in figure 7(b), at $R = 180$ and $x/d = 6$. The bursts and irregularities become more violent as R increases. It is rather difficult to determine the frequency. The Lissajous figure is unsteady because of the irregularity, but, in addition, the frequency, as well as it can be determined, varies a little. This is the reason for the scatter in this Reynolds number range. Two separate plots of $S(R)$ obtained in two different runs are shown in figure 8. They illustrate the erratic behavior of $S(R)$ in this range.

At Reynolds numbers above 300, signals like that in figure 7(c) were obtained (near the beginning of the wake). This is typical of the velocity fluctuations up to the highest value of R investigated (about 10,000). There are irregularities, but the predominant (shedding) frequency is easy to determine from a Lissajous figure. The Lissajous figure in this case is not a steady loop, as it is at $R = 40$ to 150, but neither is it so capricious as that at $R = 150$ to 300, and the matching frequency is quite easily distinguished from the nearby frequencies.

At $x/d = 48$, in this range, all traces of the periodicity have disappeared and the fluctuations are typically turbulent.

Regular and Irregular Vortex Streets

The above observations show that there are three characteristic Reynolds number ranges, within the lower end of the shedding range.

These will be called as follows:

Stable range	$40 < R < 150$
Transition range	$150 < R < 300$
Irregular range	$300 < R < 10{,}000+$

As noted above, the actual limits of these ranges are somewhat in doubt and may depend on configuration, free-stream turbulence, and so forth. Also the upper limit of the irregular range is undoubtedly higher than 10,000. (Periodic fluctuations in the wake have been observed up to the critical Reynolds number, about 200,000, but the present measurements did not extend beyond 10,000.)

In addition to the differences in the nature of the velocity fluctuations, the ranges are characterized by the behavior of the Strouhal number: In the stable range $S(R)$ is rapidly rising, in the irregular range it is essentially constant, and in the transition range it is "unstable."

It will be seen in the further results presented below that all phases of the wake development are different in the two ranges, stable and irregular, and that they are indeed two different regimes of periodic wake phenomena.

Relation of Shedding Frequency to Drag

The relation between the Strouhal number $S(R)$ and the drag coefficient $C_D(R)$ has often been noted (reference 19, p. 421). Roughly, rising values of $S(R)$ are accompanied by falling values of $C_D(R)$ and vice versa.

The relation to the form drag is even more interesting. The total drag of a cylinder is the sum of two contributions: The skin friction and the normal pressure. At Reynolds numbers in the shedding range the skin-friction drag is "dissipated" mainly in the cylinder boundary layer, while the pressure drag (or form drag) is dissipated in the wake. It may, then, be more significant to relate the shedding frequency to the form drag, both of which are separation phenomena. The R-dependence of the pressure drag coefficient C_{D_P}, taken from reference 19, page 425, is shown in figure 5. It has several interesting features:

(a) C_{D_P} is practically constant, at the value $C_{D_P} = 1$.

(b) The minimum point A is at a value of R close to that at which vortex shedding starts.

(c) The maximum point B is in the transition range.

(d) In the irregular range $C_{D_p}(R)$ is almost a "mirror reflection" of $S(R)$.

Since the drag coefficient is an "integrated" phenomenon, it is not expected to display so sharply detailed a dependence on R as does the Strouhal number, but these analogous variations are believed to be closely related to the position of the boundary-layer separation point, to which both the shedding frequency and the pressure drag are quite sensitive.

Use of Shedding Frequency for Velocity Measurements

The remarkable dependence of the shedding frequency on the velocity and the possibility of accurately measuring $S(R)$ make it possible to determine flow velocities from frequency measurements in the wake of a cylinder immersed in the flow. At normal velocities the accuracy is as good as that obtainable with a conventional manometer, while at velocities below about 400 centimeters per second it is much better. (For instance, at a velocity of 50 cm/sec the manometer reading is only about 0.001 cm of alcohol.) In fact, in determining $S(R)$ in the present experiments, this method was used to measure the low velocities by measuring the shedding frequency at a second reference cylinder of large diameter. The self-consistency of this method and the agreement with Kovasznay's results are shown in figure 4.

For velocity measurements it is convenient to plot the frequency-velocity relation in terms of the dimensionless parameter F (see the section "Shedding Frequency") as has been done in figures 9 and 10. The points on these plots were taken from the best-fit line in figure 4. They are well fitted by straight lines

$$F = 0.212R - 4.5 \qquad 50 < R < 150 \tag{1a}$$

$$F = 0.212R - 2.7 \qquad 300 < R < 2000 \tag{1b}$$

which correspond to

$$S = 0.212(1 - 21.2/R) \qquad 50 < R < 150 \tag{2a}$$

$$S = 0.212(1 - 12.7/R) \qquad 300 < R < 2000 \tag{2b}$$

Line (2b) has been plotted in figure 4 to compare with what is considered the best-fit line. The agreement is better than 1 percent. If line (2b) is extended up to R = 10,000, the maximum error, relative to the best-fit line, is 4 percent.

The plot of $F(R)$ is used as follows: The shedding frequency is observed and $F = n_1 d^2/\nu$ is calculated (ν is easily determined); R is found on the $F(R)$ plot and the velocity is calculated from $R = U_o d/\nu$. Sometimes, as in the present experiments, only R is required.

Wake Energy

From the velocity traces on the oscilloscope (figs. 6 and 7) it is clear that in the regular range the fluctuating velocity $u(t)$ is purely periodic while in the irregular range some of the fluctuations are random. This difference is illustrated in figure 11 which shows the distribution of energy intensity $\overline{(u/U_o)^2}$ across the wake at two Reynolds numbers, one in the regular range, at $R = 150$, and one in the irregular range, at $R = 500$. Only half the wake is shown for each case; the one at $R = 150$ is plotted on the left side of the figure and the one for $R = 500$, on the right.

The total energy intensity $\overline{(u/U_o)^2}$ at each point was determined directly from the reading on the root-mean-square voltmeter (see the section "Electronic Equipment"). The components at the frequencies n_1 and n_2 were determined by passing the signal through the wave analyzer. The curves in each half of figure 11 satisfy the equalities

$$\overline{\left(\frac{u}{U_o}\right)^2} = \overline{\left(\frac{u_1}{U_o}\right)^2} + \overline{\left(\frac{u_2}{U_o}\right)^2} \qquad R = 150$$

$$\overline{\left(\frac{u}{U_o}\right)^2} = \overline{\left(\frac{u_1}{U_o}\right)^2} + \overline{\left(\frac{u_2}{U_o}\right)^2} + \overline{\left(\frac{u_r}{U_o}\right)^2} \qquad R = 500$$

The values of $\overline{(u/U_o)^2}$, $\overline{(u_1/U_o)^2}$, and $\overline{(u_2/U_o)^2}$ were obtained by measurement (and at $R = 150$ are self-consistent) while $\overline{(u_r/U_o)^2}$ was obtained by difference. The absolute values indicated are somewhat in doubt since the vacuum-tube voltmeter is not a true root-mean-square meter but are believed accurate to about 10 percent.

The particular feature illustrated in figure 11 (already obvious from the oscillographs) is the absence of turbulent energy at $R = 150$ as contrasted with the early appearance of turbulent energy at $R = 500$. This contrast is typical of the regular and irregular ranges.

The measurements shown were made at 6 diameters downstream, but the same features exist closer to the cylinder. In fact, fluctuations in the flow can be detected ahead of the cylinder. They display the typical characteristics in the two ranges.

Downstream Wake Development

The downstream development for the case of figure 11 (but R = 500 only) is shown in figure 12. The distribution of total energy intensity $\overline{(u/U_o)^2}$ is shown on the left of the figure and the discrete energy intensity $\overline{(u_1/U_o)^2}$, at the shedding frequency, is shown on the right. Traverses were made at 6, 12, 24, and 48 diameters downstream. The discrete energy decays quite rapidly and is no longer measurable at 48 diameters. (Note that the plot of $\overline{(u_1/U_o)^2}$ at 24 diam is shown magnified 10 times, for clarity.) A plot of $\overline{(u_2/U_o)^2}$ has not been included since it can no longer be measured at even 12 diameters. The distribution of $\overline{(u_r/U_o)^2}$ may be obtained from these curves by difference.

Figure 13 presents the downstream wake development in another way. The wake energy E was calculated by integration of curves like those in figure 12 (cf. the section "Energy"); that is,

$$E = \int_{-\infty}^{\infty} \overline{\left(\frac{u}{U_o}\right)^2}\, d\left(\frac{y}{d}\right)$$

Figure 13 is a plot of the energy ratio $(E_1 + E_2)/E$, that is, the ratio of the discrete energy relative to the total energy.

In the irregular range the energies were computed in this way at R = 500 and 4000 (two cylinder sizes in each case) and R = 2900 (one cylinder). Figure 13 shows that the decay in all these cases is similar and the wake is completely turbulent at 40 to 50 diameters.

The value of x/d for which E_1/E becomes zero was determined for a variety of cylinders, varying in size from 0.06 to 1.3 centimeters and at Reynolds numbers from 200 to 10,000. The value was found to lie between 40 and 50 in all cases but closer to 40. A precise determination is difficult (and not important) because of the asymptotic approach of E_1/E to zero (E_2 is already zero at less than 12 diam).

In contrast with this, the stable range (R = 50 and 100 in fig. 13) has no development of turbulence before 50 diameters. The plots for R = 150 and 200 illustrate the rather spectacular transition from the stable range to the irregular.

For $R = 50$ and 100 the energy ratio remained constant at unity up to $x/d = 100$. Beyond that the energy intensity is so low that the tunnel turbulence cannot be neglected.

Measurements of Spectrum

Figure 14 shows spectrum measurements at 6, 12, 24, and 48 diameters downstream at a Reynolds number of 500, in the irregular range. The lateral position y/d chosen for the measurement at each x/d is the one for which $\overline{(u_1/U_o)^2}$ is a maximum (cf. fig. 12). The method of plotting is as follows. The curve through the experimental points is the continuous spectrum $F_r(n)$, plotted in normalized coordinates. The discrete energies $F_1 = \delta(n - n_1)$ and $F_2 = \delta(n - n_2)$ are indicated by narrow "bands" which should have zero width and infinite height but are left "open" in the figure. The relative energies represented by the areas under the continuous curve and under the delta functions, respectively, are marked in the figure with values of $\overline{u_r^2/u^2}$ and $\overline{u_1^2/u^2}$, $\overline{u_2^2/u^2}$.

To normalize the continuous spectrum the dimensionless parameters $\varphi = \frac{U_o}{L} F_r(n)$ and $\eta = \frac{L}{U_o} n$ are used. In each case the curve $\varphi = \frac{4}{1 + (2\pi\eta)^2}$ is included for reference. The normalizing coefficient L was determined as follows:

(a) $F_r(0)$ was found by extrapolation of the measured values to $n = 0$.

(b) $F_r(0)$ and the other values of $F_r(n)$ were normalized to make $\int F(n)\, dn = 1$.

(c) L was found from $\frac{U_o}{L} F_r(0) = 4$.

In short, the measured curve and the reference curve were made to agree in $\varphi_r(0)$ and in area. This requirement determines L.

In these coordinates the shedding frequency shows an apparent increase downstream; this is because the normalizing parameter L increases. For $x/d = 48$ the shedding frequency (i.e., n_1) is marked with a dash; it contains no discrete energy at this value of x/d.

The "bumps" in the continuous spectrum, near n_1 and n_2, indicate a feeding of energy from the discrete to the continuous spectrum. The portion of the spectrum near $n = 0$, which is established early and which contains a large part of the turbulent energy, seems to be unrelated to the shedding frequency (cf. fig. 15). As the wake develops the energy in the bumps is rapidly redistributed (part of it decays) to smooth the spectrum, which, in the fully developed turbulent wake at 48 diameters, tends toward the characteristic curve $\varphi = \frac{4}{1 + (2\pi\eta)^2}$.

In figure 16 the spectrum for $x/d = 12$ and $y/d = 0.8$ is plotted together with the one at $y/d = 0$. The curves are similar at low frequencies (large eddies) and at high frequencies; they differ only in the neighborhood of the discrete band. (The slight discrepancy between this figure and fig. 14 is due to the fact that they were measured at two different times, when the kinematic viscosity ν differed. This resulted in different values of n_1 at the same R.)

A similar downstream development is shown in figure 15 for $R = 4000$. Here the spectrum at $x/d = 6$ is smoother than that in the previous example (fig. 14). This effect may be due not so much to the higher Reynolds number as to the fact that the shedding frequency is closer to the low frequencies; that is, the shedding frequency is "embedded" in the low-frequency turbulent band. It seems to result, at 48 diameters, in a much closer approach to the reference curve.

Figure 17 shows the spectra at 48 diameters for three cylinders and several values of y/d. It is remarkable that $R = 4000$, $d = 0.477$ cm agrees better with $R = 500$, $d = 0.190$ cm than with $R = 4000$, $d = 0.953$ cm. This seems to bear out the above remark about the relative influence of R and n_1, for the respective shedding frequencies are 565, 440, and 144.

Finally it may be noted that values of $\overline{u_r^2}$, which in figure 11 were obtained by difference, check well with the values computed from $\overline{u_r^2} = \int F_r(n)\, dn$ (before normalization of $F_r(n)$).

Spectra for the regular range are not presented, for they are simple discrete spectra.

Spanwise Correlation and Phase Measurements

The function R_z was not measured, but the main features of the spanwise correlation[4] are illustrated in figures 7 and 18.

Figure 7 shows three examples, in each of which simultaneous signals were obtained from two hot-wires at $x/d = 6$ and $y/d = 1$ and separated by 50 diameters spanwise. The two signals were obtained simultaneously on the oscilloscope screen by means of an electronic switch. This accounts for the dotted traces.

At $R = 145$ (fig. 7(a)) the correlation is perfect but there is a phase shift. At $R = 180$ (fig. 7(b)) the correlation is still good but the individual signals occasionally break down. The breakdowns are uncorrelated at this distance of 50 diameters. At $R = 500$ (fig. 7(c)) each signal still shows a predominant frequency. There is some variation in phase between the two signals. The amplitude irregularities appear to be uncorrelated.

Figure 18 shows the correlation figures obtained by placing the signals of the two hot-wires on the horizontal and vertical plates, respectively, of the oscilloscope.

For $R = 80$ and $\zeta/d = 100$ a steady Lissajous figure is obtained, showing that the periodic fluctuations at the two points (100 diam apart) are perfectly correlated (but they are not in phase).

For $R = 220$ and 500 there is good correlation only at small values of ζ/d, that is, only when the two hot-wires are in the same "eddy," so to speak. For $R = 500$ the figures are similar to those obtained in fully developed turbulence.

In obtaining these correlations a remarkable phenomenon was observed. The stable vortex street (that is, $R < 150$) has a periodic spanwise structure. This was shown by the phase shifts on the Lissajous figure, as the movable hot-wire was traversed parallel to the cylinder. From the phase coincidences observed, the wave length parallel to the cylinder was about 18 diameters at a Reynolds number of 80. It has not been determined whether this periodicity structure is due to a "waviness" in the vortex filaments or whether the vortex filaments are straight but inclined to the cylinder axis.

---

[4]In the remainder of this section a distinction is made between the terms "correlation function" and "correlation." The former refers to the function defined in the section "Space correlation function; phase relations" while the latter is used in a looser, descriptive sense.

Statistical Measurements

A few amplitude distribution functions were measured and are shown in figure 19. One measurement is in the stable range; the other shows downstream development in the irregular range.

The table in figure 19 shows values of c and α computed from these curves. The behavior, of course, is as expected, but the numerical values are of some interest. These values (and the curves) show that at $R = 100$ the signal was practically triangular but had rounded "tops," At $R = 500$ the downstream development of randomness is shown by the tendency of c and α toward the Gaussian values.

The distribution is in fact not Gaussian, as may be seen in the figure, for its skewness σ is quite high.

Vortex Rings

The flow behind wire rings was briefly investigated. The dimensions of the rings used are given in table II.

With the rings of diameter ratio $D/d = 10$ vortices are shed from the wire in almost the same way as from the straight wire, and there is apparently an annular vortex street for some distance downstream. The Strouhal number, measured from $R = 70$ to 500, is lower than that for the straight wire (about 3 percent at $R = 500$ and 6 percent at $R = 100$).

Fluctuating velocity amplitudes were measured in the wake at several downstream positions. The results for the largest ring, measured along a diameter, are shown in figure 20. It should be noted that $\sqrt{\overline{u^2}}$ rather than the energy has been plotted here (cf. fig. 11); only relative values were computed. Close behind the cylinder the wake behind the wire on each side of the ring is similar to that behind the straight wire, but the inside peaks are lower than the outside peaks. This may be partly due to the interference of the hot-wire probe, for a similar effect, much less pronounced, was noticed in the measurements behind a straight wire.

Farther downstream there was some indication of strong interaction between the vortices, for a peak could not be followed "smoothly" downstream. However, the investigations were not continued far enough to reach conclusive results. At about 40 diameters downstream the flow became unstable.

The ring with $D/d = 5$ behaved somewhat differently. The observed frequencies gave values of Strouhal number as shown in table III. The table shows values of S and R based on the wire diameter, as well as values of S_D and R_D based on ring diameter. Between $R = 153$ and 182 there is a sudden increase in S, and at higher Reynolds numbers, in what corresponds to the irregular range, the shedding is similar to that from a straight wire, while in the stable range the shedding is at a much lower frequency. From the observations made it seems likely that in the stable range the ring acts like a disk, shedding the vortex loops observed by Stanton and Marshall (reference 18, p. 578, and reference 20). Stanton and Marshal do not give their frequency-velocity observations except at the critical R_D, where shedding first starts. They observed this to be at about $R_D = 200$, with a corresponding S_D of 0.12.

Again, these experiments were too incomplete to warrant definite conclusions, but the difference in behavior for $D/d = 10$ and $D/d = 5$ is interesting. This behavior is similar to that observed by Spivack (reference 21) in his investigation of the frequencies in the wake of a pair of cylinders which were separated, normal to the flow, by a gap. He found that when the gap was just smaller than 1 diameter instability occurred. For larger gaps the cylinders behaved like individual bodies, while for smaller gaps the main frequencies were, roughly, those corresponding to a single bluff body of dimension equal to that of the combined pair, including the gap.

DISCUSSION

The most significant results of this investigation may be discussed in terms of the Reynolds number ranges defined in the section "Regular and Irregular Vortex Streets," namely, the stable range from $R = 40$ to 150, the transition range from $R = 150$ to 300, and the irregular range above $R = 300$.

Stability

The transition range from $R = 150$ to 300 displays the characteristics of a laminar-turbulent transition, and it is instructive to compare the stability of the flow around the cylinder with boundary-layer stability. The flow in the irregular range has turbulent characteristics, while in the stable range it is essentially viscous.

The Reynolds number regimes may be described as follows: Below $R = 40$ the flow around the cylinder is a symmetric, viscous configuration, with a pair of standing vortices behind the cylinder. At about $R = 40$ this symmetric configuration becomes unstable. It changes to a

new, stable configuration which consists of alternate periodic breaking away of the vortices and formation of a regular vortex street. The instability at $R = 40$ is not a laminar-turbulent instability; it divides two different ranges of stable, viscous flow. In either range, disturbances to the stable configuration will be damped out.

On the other hand, the transition range from $R = 150$ to 300 involves a laminar-turbulent transition. To understand how this transition is related to the vortex shedding, it is necessary to know something about the formation of the vortices. Involved in this formation is the circulating motion behind the cylinder as shown in the following sketch. A free vortex layer (the separated boundary layer) springs from each separation point on the cylinder. This free layer and the backflow behind the cylinder establish a circulation from which fluid "breaks away" at regular intervals.

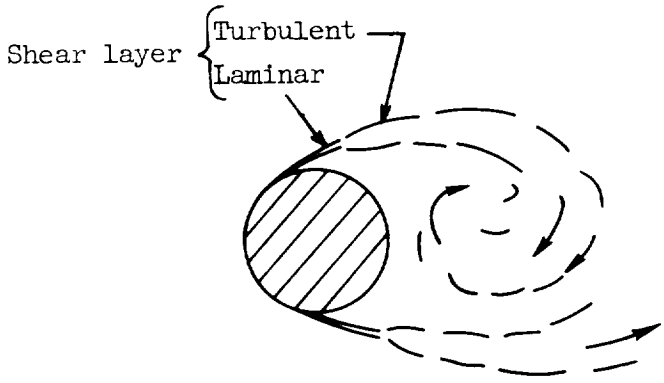

The laminar-turbulent transition is believed to occur always in the free vortex layer; that is, the circulating fluid becomes turbulent before it breaks away. Then each vortex passing downstream is composed of turbulent fluid.

The point in the free vortex layer at which the transition occurs will depend on the Reynolds number. This transition was actually observed by Schiller and Linke (reference 18, p. 555, and reference 22) whose measurements were made at cylinder Reynolds numbers from 3500 to 8500. The distance to the transition point, measured from the separation point, decreased from 1.4 diameters to 0.7 diameter, and for a given Reynolds number these distances decreased when the free-stream turbulence was increased. Dryden (reference 23) observed that at some value of R, depending on free-stream turbulence and so forth, the transition point in the layer actually reaches the separation point on the cylinder. This point then remains fixed and vortex shedding continues, essentially unchanged, up to Reynolds numbers above 100,000, that is, up to the value of R for which transition begins in the cylinder boundary layer ahead of the separation point. It is quite likely that even above this

critical value of R the phenomenon is essentially unchanged, but now the vortex layers are much nearer together and the vortices are diffused in a much shorter downstream distance.

In summary, vortex formation in the stable range occurs without laminar-turbulent transition. The circulating fluid breaks away periodically, and alternately from the two sides, forming free "viscous" vortices which move downstream and arrange themselves in the familiar vortex street. In the irregular range transition occurs in the circulating fluid before it breaks away, and the vortices are composed of turbulent fluid. The transition range corresponds to the similar range in boundary-layer stability, and it displays a similar intermittency. The values $R = 150$ and 300 used to define the range are expected to be different in other experiments, depending on wind-tunnel turbulence, cylinder roughness, and so forth.

Shedding Frequency

The Strouhal number and Reynolds number dependence is different in the two ranges. In the stable range $S(R)$ is rapidly rising, while in the irregular range it is practically constant.

Fage and Johansen, who investigated the structure of the free vortex layers springing from the separation points on various bluff cylinders (reference 9), made an interesting observation on the relation of the shedding frequency to the distance between the vortex layers. This distance increases as the cylinder becomes more bluff, while the shedding frequency decreases. In fact, if a new Strouhal number S' is defined in terms of the distance d' between the free vortex layers (instead of the cylinder dimension d), then a universal value $S' \approx 0.28$ is obtained for a variety of (bluff) cylinder shapes. The measurements of reference 9 were made at $R = 20{,}000$, but it is believed that the similarity exists over the whole irregular range. It does not extend to the stable range. To check this point the shedding frequency was measured in the wake of a half cylinder placed with the flat face broadside to the flow. It was found that $S(R)$ was rising for Reynolds numbers below 300 and then became practically constant at the value $S = 0.140$. For a similar case, at $R = 20{,}000$, Fage and Johansen found $S = 0.143$.

The universality of the constant S' is useful in systematizing the shedding phenomena (at least in the irregular range). It indicates that when the circulating fluid behind the cylinder is turbulent then the formation of free vortices is similar for a variety of bluff shapes and over a wide range of Reynolds numbers.

Finally, the relation between Strouhal number and form drag coefficient has been mentioned in the section "Relation of Shedding Frequency to Drag." In the irregular range the slight variations in $S(R)$ reflect slight variations of C_{D_P} and so, probably, of the separation point.

However, constancy of C_{D_P} is not enough to insure a fixed separation point. For instance, C_{D_P} remains practically constant down to Reynolds numbers below the shedding range, but the separation point there is farther back than it is at higher Reynolds numbers. It would seem worth while, and fairly easy, to measure the position of separation as a function of Reynolds number over the whole shedding range, that is, to complete the data available in the literature.

Downstream Development

The way in which the wake develops downstream is quite different in the stable and irregular ranges.

When the circulating fluid breaks away before the occurrence of transition in the free vortex layers (i.e., below $R = 150$) then the free vortices which are formed are the typical viscous vortices. There is no further possibility for the fluid in them to become turbulent. The vortices simply decay by viscous diffusion as they move downstream (see the section "Spread of Vortex Street" in appendix B).

When turbulent transition does occur, then the vortices which are formed consist of turbulent fluid. They diffuse rapidly as they move downstream and are soon obliterated, so that no evidence of the shedding frequency remains. This development to a completely turbulent wake takes place in less than 50 diameters. In terms of the decay of the discrete energy (fig. 13), the development is roughly the same for Reynolds numbers from 300 to 10,000. This again indicates a remarkable similarity over the whole irregular range.

The stable and irregular ranges are also characterized by the difference in the energy spectra of the velocity fluctuations. It has been pointed out that in the irregular range a continuous, or turbulent, part of the spectrum is established at the beginning of the wake development. This turbulence is a result of the transition in the free vortex layers and might be expected to be independent (at first) of the periodic part of the fluctuation, which results from the periodic shedding. Indeed, most of the energy at first is concentrated at the shedding frequency n_1 (some at n_2), and it may be represented as a discrete (delta function) part of the spectrum, within the accuracy of the measurements (cf. appendix A). However, the continuous and discrete parts are not entirely independent, as shown by the bumps near n_1 and n_2 (fig. 14). This may be regarded as a result of energy "feeding" from the discrete to the continuous parts of the spectrum, and it proceeds in a way which tends to smooth the spectrum. Such transfer of energy between spectral bands is a process depending on the nonlinear terms of the equations of motion. The "activity" in the spectrum, at any stage of its development, may be

regarded as an equilibrium between the nonlinear and the viscous terms. It is an important problem in the theory of isotropic turbulence.

The spectral activity near the frequency of discrete energy might be looked upon as a simplified case in which a single band has an excess of energy and the spectral energy flow is unidirectional, that is, out of it into the adjacent bands. However, the nonhomogeneous character of the field involved (the wake) reduces the simplicity, for it is necessary to take account of energy transfer across the wake. One interesting possibility is to superimpose a homogeneous (isotropic) turbulent field, by means of a screen ahead of the shedding cylinder, and to study the effect of this field on the spectral activity near the discrete band. Although the wake will still introduce nonhomogeneity (not even counting the periodic part of the motion), it may be possible to arrange the relative magnitudes to give significant results from the simplified model.

To study such problems the technique for measuring the spectrum (appendix A) near the frequency of discrete energy will be improved.

To summarize, it is suggested that the initial development of the spectrum might be regarded as follows. The continuous and the discrete parts are established independently, the one by the transition in the vortex layers and the other by the periodic shedding. The turbulence due to the transition is the "primary" turbulent field and its spectrum is the typical, continuous (turbulent) spectrum. (It has been noted in the section "Measurements of Spectrum" that the low-frequency end of the spectrum is established early; it would contain only energy of the primary field.[5]) The discrete part of the spectrum is embedded in the turbulent part, and it thereby is "excited" into spectral transfer. Some of its energy is transferred to the adjacent frequency bands resulting, initially, in the development of bumps in the continuous spectrum. Subsequently, as the spectral transfer proceeds, the spectrum becomes smooth.

The above discussion is an abstract way of saying that the vortices are diffused by a turbulent fluid (instead of a viscous one). The diffusion involves the nonlinear processes typical of turbulence; the study of these processes, in terms of spectrum, is an important problem.

There is a similar case of turbulent, periodic structure in the flow field between two cylinders, one of which rotates. Taylor's discovery of the periodic structure of the flow is well-known (reference 24). When the inner cylinder rotates, it is possible to obtain a steady, regular

[5]In the theory of homogeneous turbulence it is shown that the low-frequency end of the spectrum is invariant, a property related to the Loitsianski invariant.

arrangement of ring vortices, enclosing the inner cylinder, and having, alternately, opposite directions of circulation. Above a critical value of the speed of rotation this laminar, periodic structure becomes unstable and the fluid becomes turbulent, but alternate ring-shaped vortices still exist at speeds several hundred times the critical speed (reference 25).

Statistics

The probability distribution functions (fig. 19) display the characteristics which are expected, from the other observations. The contrast between the functions at $R = 100$ and $R = 500$, that is, in the stable and irregular ranges, respectively, is quite evident. In the irregular range, even at $x/d = 6$, where most of the energy is discrete, there is a marked irregularity in the fluctuation, as shown by the high value of α.

However, these descriptions are little better than qualitative, and it is hoped to obtain more interesting results by extending these statistical methods. Of particular interest in the development of random from periodic motion would be the relation between the probability distributions and the spectra. For instance, it is plain that a purely periodic function (discrete spectrum) will have a probability distribution with finite cutoff, while development of random irregularities in the function's amplitude is strongly reflected in (1) a "spreading" of the distribution function to higher values of ξ and (2) the appearance of a continuous spectrum. However, the relation between the two is not unique; that is, the spectrum does not give (complete) information about the probability distribution, and vice versa. It is not clear what the correspondence is and whether useful relationships may be obtained, possibly for restricted classes of functions.

Suggestions for Future Investigations

Some further lines of investigation indicated by these experiments are summarized below.

(a) The transition from the stable to the irregular range should be investigated with controlled disturbances, for example, cylinder roughness and free-stream turbulence. It is expected that the limits of the transition range (roughly $R = 150$ to 300 for the experimental conditions here) will be lower for higher free-stream turbulence or cylinder roughness. The critical cylinder Reynolds numbers should be related to corresponding numbers for the transition point in the free vortex layers (based on distance from separation point or on the thickness of the layer).

Such studies of stability to different disturbance amplitudes and frequencies are well-known in the case of the boundary layer. A variation of the experiments of Schubauer and Skramstad (reference 26), who used an oscillating wire in the boundary layer to produce disturbances of definite frequencies, would be to use a second shedding cylinder.

(b) A study of the spectral development in the neighborhood of a discrete band, the effect of a turbulent field on its activity, and so forth (discussed in the section "Downstream Development") may be the most fruitful continuation of these experiments. So far, the problem has been approached only in the theory of isotropic turbulence, where it has not advanced much beyond the similarity considerations of Kolmogoroff, and very little is known about the form of the spectral transfer function.

Interactions between discrete bands, for example, at slightly different frequencies, can be studied by the use of two or more cylinders arranged to "interfere" with each other (some such studies have been made by Spivack (reference 21) but not from this viewpoint), or possibly by using one cylinder having diameter changes along its span.

(c) Townsend has recently used the concepts of intermittently turbulent flow and local isotropy in his investigations of the turbulent wake and has obtained a new description of its structure (reference 27). His studies were made at downstream distances of 80 diameters or more, so that the wake was fully turbulent. Probably the structure he describes is essentially the same up to the beginning of the fully developed wake (about 50 diam), but then there is the question of how it is related to the earlier developments. The most obvious "early developments" are the turbulent transition in the free vortex layers and the periodic shedding. (Although the shedding frequency is no longer distinguished far downstream, it is prominent in the early spectral developments and thus has an influence on the downstream wake.)

Such studies will involve considerably more detailed investigations of the wake structure than were made here, possibly along the lines of Townsend's experiments and the classical measurements of energy balance across the wake. The other two components of the energy $\overline{v^2}$ and $\overline{w^2}$ will be needed.

(d) The nature of the circulating flow behind the cylinder and the formation of free vortices, that is, the shedding mechanism, should receive further attention.

(e) The spanwise periodic structure of the vortex street should be investigated, beyond the very cursory observations made here. In particular, a study of the stability of single vortex filaments seems important.

(f) Measurements of the fluctuating forces on the cylinder, due to the shedding, would be interesting and should have immediate practical applications. There seems to be very little information about the magnitude of these forces. It might be obtained either by direct measurement of forces (on a segment) or pressures (with pressure pickups) or inferred from measurements of the velocity fluctuations close to the cylinder. In addition to the magnitude of the force or pressure fluctuations, their spanwise correlation is of prime importance.

CONCLUSIONS

An experimental investigation of the wake developed behind circular cylinders at Reynolds numbers from 40 to 10,000 indicated the following conclusions:

1. Periodic wake phenomena behind bluff cylinders may be classified into two distinct Reynolds number ranges (joined by a transition range). For a circular cylinder these are:

Stable range	$40 < R < 150$
Transition range	$150 < R < 300$
Irregular range	$300 < R < 10{,}000+$

In the stable range the classical, stable Kármán streets are formed; in the irregular range the periodic shedding is accompanied by irregular, or turbulent, velocity fluctuations.

2. The irregular velocity fluctuation is initiated by a laminar-turbulent transition in the free vortex layers which spring from the separation points on the cylinder. The first turbulent bursts occur in the transition range defined above.

3. In the stable range the free vortices, which move downstream, decay by viscous diffusion, and no turbulent motion is developed. In the irregular range the free vortices contain turbulent fluid and diffuse faster; the wake becomes fully turbulent in 40 to 50 diameters.

4. A velocity meter based on the relation between velocity and shedding frequency is practical.

5. In the stable range a spanwise periodic structure of the vortex street has been observed.

6. An annular vortex-street structure has been observed behind rings having a diameter ratio as low as 10.

California Institute of Technology
Pasadena, Calif., May 29, 1952

APPENDIX A

EXPERIMENTAL ANALYSIS OF SPECTRUM

These notes supplement the brief descriptions in the sections "Frequency Analyzer" and "Measurements of Spectrum."

Analyzer Response

Consider the response of a spectrum analyzer, such as that used in the present experiments, to a mixed periodic-random input, and in particular consider the problem of inferring the input from the output.

The input, an energy or power, has a random and a periodic component:

$$\overline{u^2} = \overline{u_r^2} + \overline{u_1^2} \tag{A1}$$

The corresponding spectra are defined by

$$\left.\begin{aligned} \overline{u^2} &= \overline{u^2} \int_0^\infty F(n)\, dn \\ \overline{u_r^2} &= \overline{u_r^2} \int_0^\infty F_r(n)\, dn \\ \overline{u_1^2} &= \overline{u_1^2} \int_0^\infty F_1(n)\, dn \end{aligned}\right\} \tag{A2}$$

where

$$F_1(n) = \delta(n - n_1) \tag{A3}$$

and $\delta(n)$ is the Dirac delta function.

The response characteristic of the analyzer may be obtained by considering the effect of a periodic input. When the analyzer setting n_A coincides with the input frequency n_1 the output is a maximum,

and when the setting is moved away from n_1 the output falls off. The response characteristic is

$$R(n_1 - n_A) = \frac{\text{Output at setting } n_A}{\text{Output at setting } n_A = n_1} = R(n_A - n_1) \tag{A4}$$

The output spectrum $G(n_A)$ of the analyzer is related to the input spectrum $F(n)$ by (cf. reference 15)

$$\begin{aligned} G(n_A) &= \int_0^\infty F(n)R(n - n_A)\,dn \\ &= \frac{\overline{u_r^2}}{\overline{u^2}} \int_0^\infty F_r(n)R(n - n_A)\,dn + \frac{\overline{u_1^2}}{\overline{u^2}} \int_0^\infty \delta(n_1 - n_A)R(n - n_A)\,dn \\ &= \frac{\overline{u_r^2}}{\overline{u^2}} \int_0^\infty F_r(n)R(n - n_A)\,dn + \frac{\overline{u_1^2}}{\overline{u^2}} R(n_1 - n_A) \end{aligned} \tag{A5}$$

Since $R(n - n_A)$ is sharp, that is, almost a delta function (see the section "Half Band Width," $F_r(n)$ may be considered to be constant over the significant interval of integration in equation (A5). Then

$$G(n_A) = \frac{\overline{u_r^2}}{\overline{u^2}} F_r(n_A)Q + \frac{\overline{u_1^2}}{\overline{u^2}} R(n_1 - n_A) \tag{A6}$$

where

$$Q = \int_0^\infty R(n - n_A)\,dn = \int_0^\infty R(n - n_A)\,dn_A \tag{A7}$$

is the area under the response characteristic.

Equation (A6) gives the output for a mixed periodic-random input. It is required to find the separate terms which make up this sum. The procedure is outlined in the section "Separation of Discrete Energy" below.

Half Band Width

The resolution of the analyzer is determined by its half band width ω. This is defined as the number of "cycles off resonance" at which the output falls off to 0.01 percent; that is

$$R(n_1 - \omega) = 0.0001 \tag{A8}$$

For an ideal analyzer the response characteristic would be a delta function, but even with half band widths from 30 to 145 (which is the range of the analyzer used here) the characteristic is quite sharp, relative to the frequency intervals of interest. The values 30 to 145 seem quite high, but they are a little misleading because of the high attenuation used to define ω. For example, if the response-characteristic half band width ω is 30 cycles per second it has a total width of only 6 cycles per second at 50 percent attenuation.

Separation of Discrete Energy

To separate the discrete energy $\overline{u_1^2}$ from the continuous spectrum the following procedure is used.

At $n_1 + \omega$ and $n_1 - \omega$ (see sketch) the contribution from $\overline{u_1^2}$ is

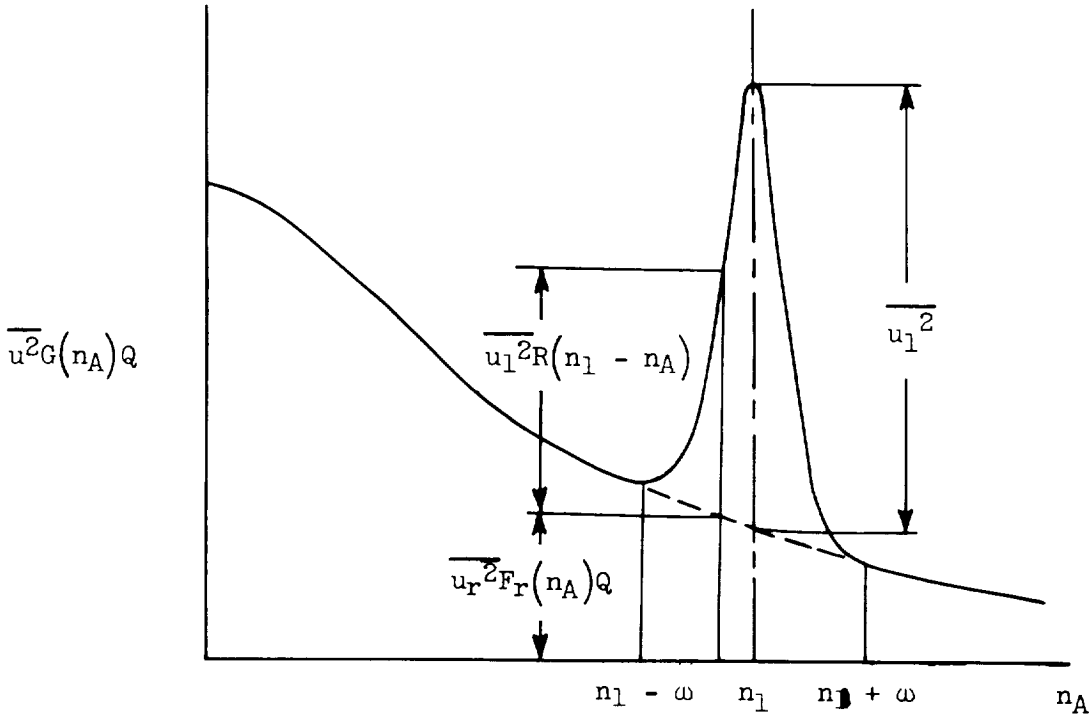

only 0.01 percent, so the measured points there are assumed to lie on the continuous spectrum. It is assumed at first that the continuous spectrum between these points may be determined by interpolation, and its value at n_1 is calculated. Then $\overline{u_1^2}$ is determined by difference and the last term in equation (A7) is calculated, since the form $R(n)$ is known. The first term in equation (A6) then gives the values of $G(n_A)$ in the vicinity of n_1; these should check the measured values.

If, however, the continuous spectrum within the band width has a bump, then the above calculation is not self-consistent, and the true values can be determined by successive estimates of $\overline{u_1^2}$.

In principle the method is satisfactory, but in practice the accuracy is low because in the regions of interest, that is, near peak frequencies, it depends on the differences of relatively large quantities. One of these, $R(n)$, is known precisely, but the precision is difficult to realize since the settings on the analyzer cannot be read accurately enough. For the spectral investigations discussed in the section "Downstream Development" the technique will be improved.

APPENDIX B

NOTES ON VORTEX-STREET GEOMETRY AND SHEDDING FREQUENCY

The regularity of the vortex shedding and its sensitivity to velocity changes have undoubtedly intrigued everyone who has investigated the flow past bluff bodies. However, as Kármán pointed out in his first papers on the vortex street, the problem is inherently difficult, involving as it does the separation of the boundary layer from the cylinder, and there is yet no adequate theoretical treatment of the mechanism.

The following notes may be useful as a summary of the interesting features of the problem. They are based largely on the literature but include some results obtained during the present experiments. Chapter XIII of reference 19 has a very useful review and list of references.

Idealized Kármán Street

Kármán's theory treats a double row of potential vortices, infinite in both directions. The distance between the rows h and the spacing of the vortices in each row l are constants. The vortices have strength (circulation) Γ which, with the geometry, determines the velocity V of the street relative to the fluid. The theory shows that the configuration is stable when the rows are staggered by a half wave length and the spacing ratio is

$$\frac{h}{l} = 0.281 \tag{B1}$$

The circulation and velocity relative to the fluid are then related by

$$\frac{\Gamma}{Vl} = 2.83 \tag{B2}$$

Two of the parameters (h, l, Γ, and V) must be determined from some other considerations. In the real vortex street they must be related to the conditions at the cylinder.

Real Vortex Street

The real vortex street, even in the stable range, differs from the idealized one in the following points:

(1) The street is not infinite. It starts shortly downstream of the cylinder and eventually loses its identity far downstream. However, the classical vortex-street patterns extending for 10 or more wave lengths should be a good approximation.

(2) The vortex spacing is not constant. In particular, the lateral spacing h increases downstream.

(3) The real vortices must have cores of finite radius. These grow downstream, so that the vortices diffuse into each other and decrease their circulation. For the same reason the velocity V is expected to differ considerably from the theoretical value, since it is strongly dependent on the configuration.

Related to these considerations is the way in which the vortices are first formed. At Reynolds numbers below the shedding range a symmetrical pair of eddies is formed at the back of the cylinder. As the Reynolds number increases these two eddies grow and become more and more elongated in the flow direction, until the configuration is no longer stable and becomes asymmetric. Once this occurs the circulating fluid breaks away[6] alternately from each side to form free vortices which flow downstream and arrange themselves into the regular, stable vortex street.

In the irregular range the process is similar, except that the fluid is turbulent (because of the transition in the free vortex layers).

Downstream Vortex Spacing

In the flow past a stationary cylinder the frequency with which vortices of one row pass any point is given by

$$n_1 = \frac{U_o - V}{l} \tag{B3}$$

This must be the same as the shedding frequency

$$n_1 = SU_o/d \tag{B4}$$

Two useful expressions result:

$$\frac{l}{d} = \frac{1}{S}\left(1 - \frac{V}{U_o}\right) \tag{B5}$$

[6]Possibly the breaking away should be regarded as primary, resulting in asymmetry.

or

$$\frac{V}{U_o} = 1 - \frac{Sl}{d} \tag{B6}$$

In a real vortex street, $V \longrightarrow 0$ far downstream and then $\frac{l}{d} \longrightarrow \frac{1}{S}$. Or, if Sl/d is known from measurements, then V/U_o may be computed.

An example of measured values of l/d is shown in figure 21. These were taken from the streamline plot obtained by Kovasznay (reference 11) at $R = 53$ (for which $S = 0.128$). There is a little scatter but l/d does approach the constant value $1/S = 7.8$.

The scatter, while relatively unimportant in the case of l/d, gives very low accuracy for values of V/U_o calculated from equation (B6). These have also been plotted in figure 21. It is surprising that some of the values, near the cylinder, are negative (corresponding to values of l/d higher than $1/S$); it is believed that this results from the combined difficulty of estimating the vortex centers, especially near the cylinder, and the sensitivity of equation (B6). (However, it must be noted that negative values of V are not impossible. Negative V simply means that the vortex velocity is directed upstream relative to the fluid, while it is still downstream relative to the cylinder. Such a possibility exists at low values of x/d, where the mean velocity at the edges of the wake is considerably higher than U_o.)

Another way to obtain V/U_o is to assume that the vortex centers move with the local mean velocity. Kovasznay's paper includes measurements of mean velocity profiles. From his results the mean velocity along the line of vortex centers U^* has been determined and from it $\frac{V}{U_o} = 1 - \frac{U^*}{U_o}$ has been calculated. The result is plotted in figure 21. Near the cylinder it does not agree with the values obtained by the previous method; it is believed that this is principally due to the difficulties mentioned above and that the determination of V/U_o from $1 - (U^*/U_o)$ is more accurate.

Lateral Spacing

The lateral spacing, at least initially, must be determined by conditions near the cylinder. The way in which this spacing increases downstream is discussed, for the stable range, in the section "Spread of Vortex Street."

In the irregular range, the dependence of the shedding frequency on the distance between the free vortex layers, noted by Fage and Johansen (see the section "Shedding Frequency"), leads to an interesting estimate of the initial lateral spacing of the free vortices. The maximum distance d' between the free vortex layers, instead of the cylinder dimension d, may be used to define a new Strouhal number

$$S' = n_1 \frac{d'}{U_o} \tag{B7}$$

Fage and Johansen found that, whereas S varies considerably with cylinder shape, S' is practically constant for a variety of bluff cylinders. Now the initial lateral spacing h' of the free vortices will be roughly the same as d', possibly a little smaller:

$$\frac{h'}{l} = (1 - \epsilon)\frac{d'}{l} \tag{B8}$$

Then, comparing with equations (B6) and (B7),

$$\frac{h'}{l} = \frac{1 - \epsilon}{1 - (V/U_o)} S' \tag{B9}$$

From the measurements of Fage and Johansen, $S' \approx 0.28$. The factor $\frac{1 - \epsilon}{1 - (V/U_o)} \approx 1$. Thus equation (B9) gives $h'/l = 0.28$; that is, the spacing ratio agrees with Kármán's value, at least close to the cylinder.

Shedding Frequency

There is yet no adequate theory of the periodic vortex shedding, and it is not clear what is the principal mechanism which determines the frequency.

The downstream spacing ratio is related to the shedding frequency by equation (B3) and to the lateral spacing by a stability criterion (e.g., Kármán's value of 0.28 for the idealized street). It might be considered that the shedding frequency is determined by the spacing requirement, or, conversely, that the shedding is primary and determines the downstream spacing. The latter viewpoint seems the more plausible one; that is, the shedding frequency is established by a mechanism which depends on features other than the vortex spacing. It is necessary to

obtain a better understanding of the flow field near the cylinder. One of the elements involves the problem of separation, particularly the nonstationary problem. Another that requires more study is the flow field directly behind the cylinder.

With a better knowledge of these, and possibly other, features it may be possible to set up a model of the shedding mechanism. In the meantime it is not clear whether the vortex spacing requirement is decisive in determining the frequency.

Destabilization[7] of Shedding

The following experiment illustrates the dependence of the periodic shedding on "communication" between the free vortex layers, that is, on the flow field directly behind the cylinder. A thin flat plate was mounted behind the cylinder in the center plane of the wake (fig. 22). It was completely effective in stopping the periodic shedding. Spectrum measurements in the flow on one side of the plate are shown in figure 22. At $R = 7500$ no significant frequencies could be separated out from the continuous background. At $R = 3200$ there were several predominant frequencies (all higher than the shedding frequency for the cylinder), but, by the time the flow reached the end of the plate, 5 diameters downstream, it was completely turbulent. (The shedding frequency n_1 for the cylinder is marked in the figures.)

The important effect, on the shedding, of the flow field directly behind the cylinder is apparent. Probably an even shorter length of plate would be effective in destabilizing the periodic shedding, and there may be a most effective position for such an interference element. Kovasznay remarks that the hot-wire probe used in investigating the vortex street must be inserted from the side, for if it lies in the plane of the street it has a strong destabilizing influence.

A more complete study of the destabilization of shedding by such interference devices may be quite useful from a practical viewpoint. Structural vibrations and failures are often attributed to the periodic forces set up on members exposed to wind or other flow (smokestacks, pipe lines, structural columns, to mention a few). In many cases it might be possible to destabilize the vortex shedding by addition of simple interference elements or by incorporating them in the original designs. In the case where one member is buffeted by the wake of another the same principle might be applied.

---

[7]The stability considered in this section is not with respect to laminar-turbulent transition; it concerns the stability of the periodic shedding (cf. the section "Stability").

Spread of Vortex Street

It has been observed by most investigators that the spacing ratio h/l is Kármán's value (0.28) close to the cylinder but increases rapidly downstream. The increase of h/l is mainly due to the increase of h, since l changes very little (fig. 21). In the stable range this is the result of viscous diffusion of the real vortices.

Hooker (reference 28) has made an interesting analysis. First, a real vortex has a core of finite radius; its center is the point of zero velocity and maximum vorticity. Hooker shows that in a vortex street, where the velocity field of the other vortices must be taken into account, the points of zero velocity and maximum vorticity do not coincide. The point of maximum vorticity is unchanged but the point of zero velocity is farther away from the center of the street. As the vortex decays, the point of zero velocity moves farther out, its distance from the center of the street increasing almost linearly with time. Thus the spacing based on vorticity centers remains constant, while the spacing based on velocity centers increases linearly. Hooker's calculation of the linear spread checks fairly well with some pictures taken by Richards (reference 29) in the wake of an elliptical cylinder having a fineness ratio of 6:1 and the major diameter parallel to the free-stream velocity.

However, the spread of the wake is not always observed to be linear. Among the different investigators there is a large variation of results, apparently dependent on the experimental arrangement. In Richards' experiment the cylinder was towed in a water tank and the vortex patterns were observed on the free surface.

In Kovasznay's experiment the cylinder was mounted in a wind tunnel, the arrangement being similar to the one used here (see the section "Experimental Data"). On his plot of the streamlines at $R = 53$ the downstream spread of the vortex street is parabolic rather than linear. It is possible to fit his results by a somewhat different application of Hooker's idea, using decaying vortex filaments.

Each vortex in the street is considered to behave like a single vortex filament carried along by the fluid, its decay or diffusion being the same as if it were at rest. The decay of such a vortex is described by a heat equation, whose solution is (reference 30, p. 592):

$$q = \frac{\Gamma}{2\pi r}\left(1 - e^{-r^2/4\nu t}\right) \tag{B10}$$

where q is the tangential velocity at the distance r from the center and at the time t. The circulation is Γ. This is essentially a vortex with a "solid" core and potential outer flow joined by a transition

region in which the velocity has a maximum value. This maximum velocity is

$$q^* = 0.72(\Gamma/2\pi r^*) \tag{B11}$$

and occurs at the radial distance

$$r^* = 2.24(\nu t)^{1/2} \tag{B12}$$

Here r^* is defined as the vortex radius.

Thus the radius increases as $t^{1/2}$ and the maximum velocity decreases as $t^{-1/2}$. In the vortex street, the time t is replaced by the downstream distance x. Since the vortices move with the velocity U^* rather than U_o, the dimensionless time $\theta = \frac{U_o}{U^*}\frac{x}{d}$ is appropriate, where U^* also varies downstream (see the section "Downstream Vortex Spacing").

When a pattern of such vortices is superimposed on a uniform flow, it is possible to calculate the velocity fluctuation at a point, because of the pattern passing over it.

Now the following hypothesis is added. It is assumed that the vortex radius r^* is equal to the width h of the street. Then the width of the street increases as $x^{1/2}$.

A second result follows. The maximum velocity fluctuation (observed by a hot-wire, say) will occur <u>on the line of vortex centers</u> and will have the amplitude

$$u^* = \frac{1}{2} q^* \tag{B13}$$

that is, the hot-wire encounters instantaneous velocities varying from U^* (because of vortex centers passing over it) to $U^* + q^*$ (due to the fields of vortices on the other side of the street). Relations (B11) and (B12) then give the downstream behavior of the maximum fluctuation amplitude.

The results may be summarized as follows:

(a) Wake width $h \approx \theta^{1/2}$.

(b) The maximum amplitude of fluctuation u^* occurs on the line of vortex centers (so there are two maximum points across the wake).

(c) $u^* \approx \theta^{-1/2}$.

(d) $u^* = 0.36(\Gamma/2\pi h)$.

A comparison of the above predictions was made with calculations based on Kovasznay's measurements which include profiles of velocity fluctuation amplitude (cf. fig. 11) as well as the streamline plot. The following comparisons were obtained, item by item:

(a') The time variation of h/d, determined from the vortex centers on the streamline plot is shown in figure 21. The parabola $h/d = 0.59(\theta - 6)^{1/2}$ is shown for comparison.

(b') The line of maximum velocity fluctuation lies slightly inside the line of vortex centers and is fitted by $h^*/d = 0.53(\theta - 6)^{1/2}$.

(c') The time variation of u^* is also plotted in figure 21. (Actually Kovasznay's maximum root-mean-square values u'_m are plotted, but these should differ from u^* only by a constant factor.) The curve $u'_m/U_o = 0.26(\theta - 6)^{-1/2}$ is shown for comparison. The points could be fitted better, but the curve was chosen again to have the origin $\theta = 6$.

(d') A comparison with (d) may be made by estimating the strength Γ of the vortices. Such a consideration, in fact, led to the present model, for it was found that the magnitude of the observed velocity fluctuations could be accounted for only by assuming that the radius of the vortex core is about equal to the width of the street. This observation had already been made by Fage and Johansen (reference 8), for $R \approx 2 \times 10^4$. If the free vortex layer is represented by a velocity discontinuity $U = U_o$ to $U = 0$ then the circulation is U_o per unit length and "the circulation" flows with the velocity $U_o/2$. On the other hand, the rate at which circulation enters one side of the street is $n_1\Gamma$, where Γ is the circulation per vortex.[8] Therefore

$$\Gamma = \frac{U_o^2}{2n_1} = \frac{U_o d}{2S}$$

For Kovasznay's example, $S \approx 0.13$, so $\Gamma \approx 4U_o d$. Then, comparing with (d), the maximum fluctuation in the initial part of the wake is

---

[8]The velocity at the outer edge of the layer is actually about $1.5U_o$, but experiments indicate that only about half the vorticity of the shear layer goes into individual vortices. Therefore, the value $U_o d/2S$ is a fair estimate.

$$\frac{u^*}{U_o} \approx 0.2 \frac{d}{h} = 0.2$$

assuming $h \approx d$ at this low Reynolds number. The largest value of u'_m/U_o in Kovasznay's example is 0.14 at $x/d = 7$, corresponding to $u^*/U_o \approx 2$. The order of magnitude of this estimate is quite sensitive to the size of the core relative to the width of the street; if the core is assumed to be much smaller, the calculated velocity fluctuations are much larger than those observed. Also, if the cores were very small compared with the width of the wake, four peaks instead of two would be observed in the profile of the velocity fluctuation amplitude.

REFERENCES

1. Strouhal, V.: Über eine besondere Art der Tonerregung. Ann. Phys. und Chemie, Neue Folge, Bd. 5, Heft 10, Oct. 1878, pp. 216-251.

2. Rayleigh, Lord: The Theory of Sound. Vol. II. Dover Publications, 1945.

3. Rayleigh, Lord: Acoustical Observations. Phil. Mag., ser. 5, vol. 7, no. 42, March 1879, pp. 149-162.

4. Flachsbart, O.: Geschichte der experimentellen Hydro- und Aeromechanik, insbesondere der Widerstandsforschung. Bd. 4, Teil 2 der Handbuch der Experimentalphysik, Ludwig Schiller, ed., Akademische Verlags G.m.b.H. (Leipzig), 1932, pp. 3-61.

5. Ahlborn, F.: Über den Mechanismus des Hydro-dynamischen Widerstandes. Abh. Geb. Naturwiss., Bd. 17, 1902.

6. Benard, H.: Formation de centres de giration à l'arrière d'un obstacle en mouvement. Comp. rend., Acad. Sci. (Paris), t. 147, Nov. 9, 1908, pp. 839-842.

7. Von Kármán, Th., and Rubach, H.: Über den Mechanismus des Flussigkeits und Luftwiderstandes. Phys. Zeitschr., Bd. 13, Heft 2, Jan. 15, 1912, pp. 49-59.

8. Fage, A., and Johansen, F. C.: On the Flow of Air behind an Inclined Flat Plate of Infinite Span. R. & M. No. 1104, British A.R.C., 1927; also Proc. Roy. Soc. (London), ser. A, vol. 116, no. 773, Sept. 1, 1927, pp. 170-197.

9. Fage, A., and Johansen, F. C.: The Structure of Vortex Sheets. R. & M. No. 1143, British A.R.C., 1927; also Phil. Mag., ser. 7, vol. 5, no. 28, Feb. 1928, pp. 417-441.

10. Fage, A.: The Air Flow around a Circular Cylinder in the Region Where the Boundary Layer Separates from the Surface. R. & M. No. 1179, British A.R.C., 1928.

11. Kovasznay, L. S. G.: Hot-Wire Investigation of the Wake behind Cylinders at Low Reynolds Numbers. Proc. Roy. Soc. (London), ser. A, vol. 198, no. 1053, Aug. 15, 1949, pp. 174-190.

12. Dryden, Hugh L.: Turbulence Investigations at the National Bureau of Standards. Proc. Fifth Int. Cong. Appl. Mech. (Sept. 1938, Cambridge, Mass.), John Wiley & Sons, Inc., 1939, pp. 362-368.

13. Dryden, Hugh L.: A Review of the Statistical Theory of Turbulence. Quart. Appl. Math., vol. I, no. 1, April 1943, pp. 7-42.

14. Liepmann, H. W., Laufer, J., and Liepmann, Kate: On the Spectrum of Isotropic Turbulence. NACA TN 2473, 1951.

15. Liepmann, H. W.: An Approach to the Buffeting Problem from Turbulence Considerations. Rep. No. SM-13940, Douglas Aircraft Co., Inc., March 13, 1951.

16. Liepmann, Hans Wolfgang, and Laufer, John: Investigations of Free Turbulent Mixing. NACA TN 1257, 1947.

17. Liepmann, H. W., and Robinson, M. S.: Counting Methods and Equipment for Mean Value Measurements in Turbulence Research. NACA TN to be published.

18. Robinson, M.: Ten-Channel Statistical Analyzer for Use in Turbulence Research. Aero. Eng. Thesis, C.I.T., 1952.

19. Fluid Motion Panel of the Aeronautical Research Committee and Others (S. Goldstein, ed.): Modern Developments in Fluid Dynamics. Vol. II. The Clarendon Press (Oxford), 1938.

20. Stanton, T. E., and Marshall, Dorothy: On the Eddy System in the Wake of Flat Circular Plates in Three Dimensional Flow. R. & M. No. 1358, British A.R.C., 1930; also Proc. Roy. Soc. (London), ser. A, vol. 130, no. 813, Jan. 1, 1931, pp. 295-301.

21. Spivack, Hermann N.: Vortex Frequency and Flow Pattern in the Wake of Two Parallel Cylinders at Varied Spacing Normal to an Air Stream. Jour. Aero. Sci., vol. 13, no. 6, June 1946, pp. 289-301.

22. Schiller, L., and Linke, W.: Druck- und Reibungswiderstand des Zylinders bei Reynoldsschen Zahlen 5000 bis 40000. Z.F.M., Jahrg. 24, Nr. 7, April 13, 1933, pp. 193-198. (Available in English translation as NACA TM 715.)

23. Dryden, Hugh L.: The Role of Transition from Laminar to Turbulent Flow in Fluid Mechanics. Bicentennial Conference, Univ. of Penn., Univ. of Penn. Press (Philadelphia), 1941, pp. 1-13.

24. Taylor, G. I.: Stability of a Viscous Liquid Contained between Two Rotating Cylinders. Phil. Trans. Roy. Soc. (London), ser. A, vol. 223, no. 612, Feb. 8, 1923, pp. 289-343.

25. Pai Shih-I: On Turbulent Flow Between Rotating Cylinders. Ph. D. Thesis, C.I.T., 1939.

26. Schubauer, G. B., and Skramstad, H. K.: Laminar Boundary-Layer Oscillations and Stability of Laminar Flow. Jour. Aero. Sci., vol. 14, no. 2, Feb. 1947, pp. 69-78.

27. Townsend, A. A.: Momentum and Energy Diffusion in the Turbulent Wake of a Cylinder. Proc. Roy. Soc. (London), ser. A, vol. 197, no. 1048, May 11, 1949, pp. 124-140.

28. Hooker, S. G.: On the Action of Viscosity in Increasing the Spacing Ratio of a Vortex Street. Proc. Roy. Soc. (London), ser. A, vol. 154, no. 881, March 2, 1936, pp. 67-89.

29. Richards, G. J.: An Experimental Investigation of the Wake behind an Elliptic Cylinder. R. & M. No. 1590, British A.R.C., 1933; also Phil. Trans. Roy Soc. (London), ser. A, vol. 233, no. 726, July 18, 1934, pp. 279-301.

30. Lamb, Horace: Hydrodynamics. Sixth ed., Dover Publications, 1945.

TABLE I

PROBABILITY FUNCTIONS

u(t)	p(ξ)	P(ξ)	N_k	c	α
Random function (Gaussian)	$\frac{2}{\sqrt{\pi}} e^{-\xi^2}$ $\quad -\infty < \xi < \infty$	$\frac{1}{2}(1 + \operatorname{erf} \xi)$ $\quad \xi \leq 0$ $\frac{1}{2}(1 - \operatorname{erf} \xi)$ $\quad \xi \geq 0$	$\frac{1.3 \cdot \cdot \cdot (2k - 1)}{2^k}$ k even $\frac{1}{\sqrt{\pi}} \Gamma\left(\frac{k + 1}{2}\right)$ k odd	$\sqrt{\frac{\pi}{2}} = 1.25$	3
Triangular wave	$\sqrt{\frac{2}{3}}$ $\quad \lvert\xi\rvert \leq \sqrt{\frac{3}{2}}$	$\frac{1}{2} - \frac{\xi}{\sqrt{6}}$	$\frac{1}{k + 1}\left(\frac{3}{2}\right)^{k/2}$	$\frac{2}{\sqrt{3}} = 1.16$	9/5
Sine wave	$\frac{1}{\pi\sqrt{1 - \xi^2}}$ $\quad \lvert\xi\rvert \leq 1$	$\frac{1}{\pi} \cos^{-1} \xi$	$\frac{1}{\sqrt{\pi}} \frac{\Gamma\left(\frac{k + 1}{2}\right)}{\Gamma\left(\frac{k}{2} + 1\right)}$	$\frac{\pi}{2\sqrt{2}} = 1.11$	3/2
Square wave	$\frac{1}{2} \delta\left(\lvert\xi\rvert - \frac{1}{\sqrt{2}}\right)$	$1, \ \xi < -\frac{1}{\sqrt{2}}$ $\frac{1}{2}, \ -\frac{1}{\sqrt{2}} < \xi < \frac{1}{\sqrt{2}}$ $0, \ \xi > \frac{1}{\sqrt{2}}$	$\left(\frac{1}{2}\right)^{k/2}$	1	1

TABLE II

RING DIMENSIONS

Ring	d (cm)	D	d_s	D/d
1	0.168	1.59	0.030	9.5
2	.081	.81	.018	10.0
3	.079	.40	.018	5.1

NACA

TABLE III

VALUES OF STROUHAL NUMBER FOR VARIOUS TEST

REYNOLDS NUMBERS

R	S	R_D	S_D
89	0.051	450	0.26
96	.052	490	.265
103	.052	525	.265
128	.057	650	.29
153	.060	780	.31
182	.147		
215	.189		
302	.204		
366	.211		
455	.212		

NACA

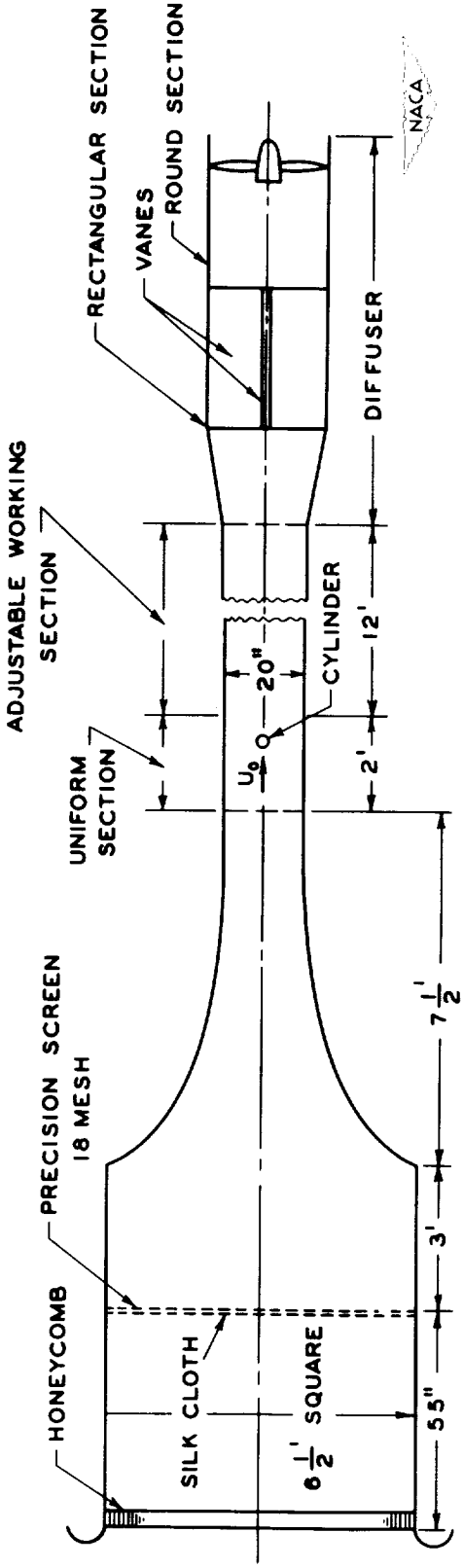

Figure 1.- Sketch of GALCIT 20-inch tunnel.

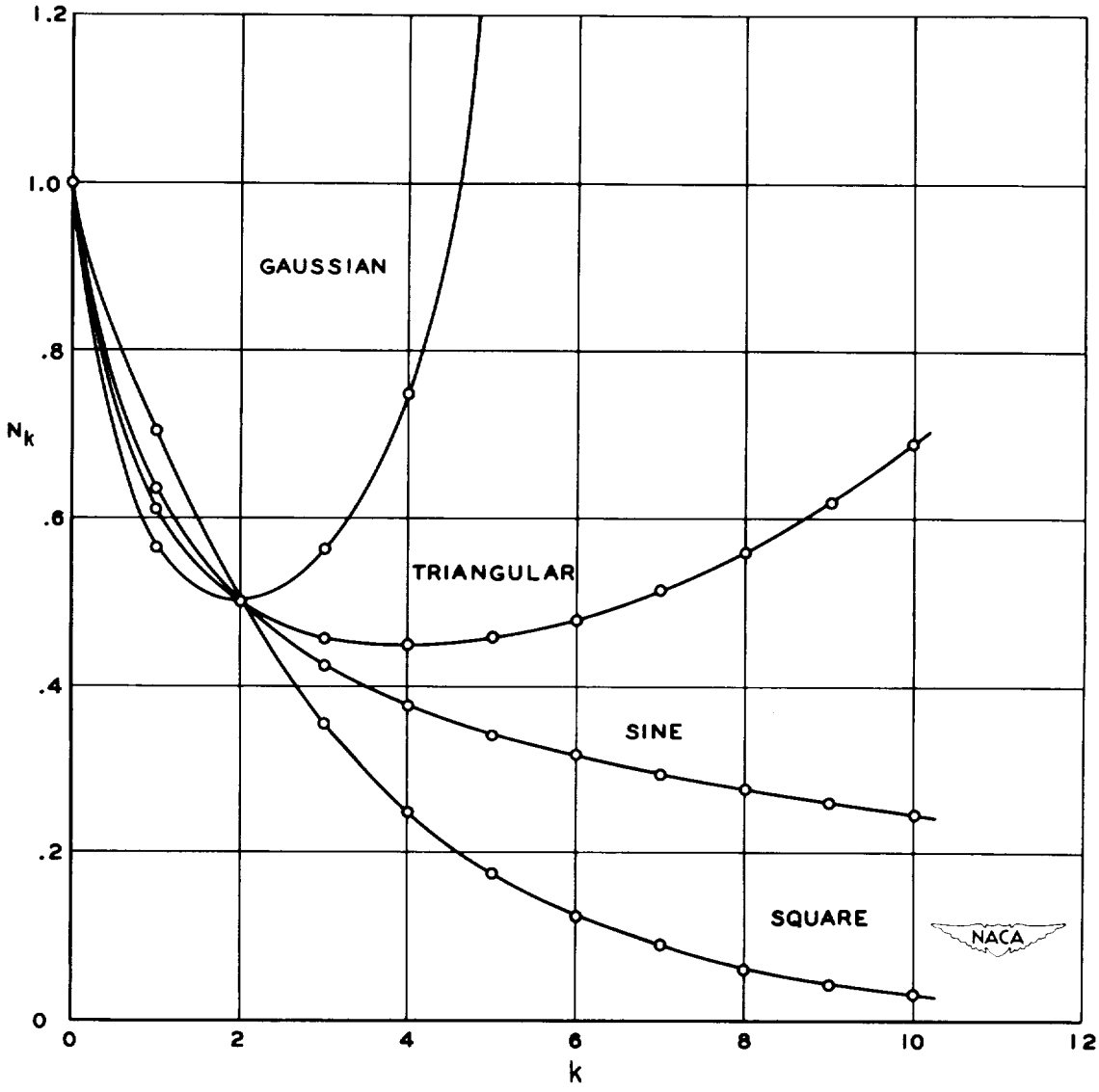

Figure 2.- Amplitude distribution moments.

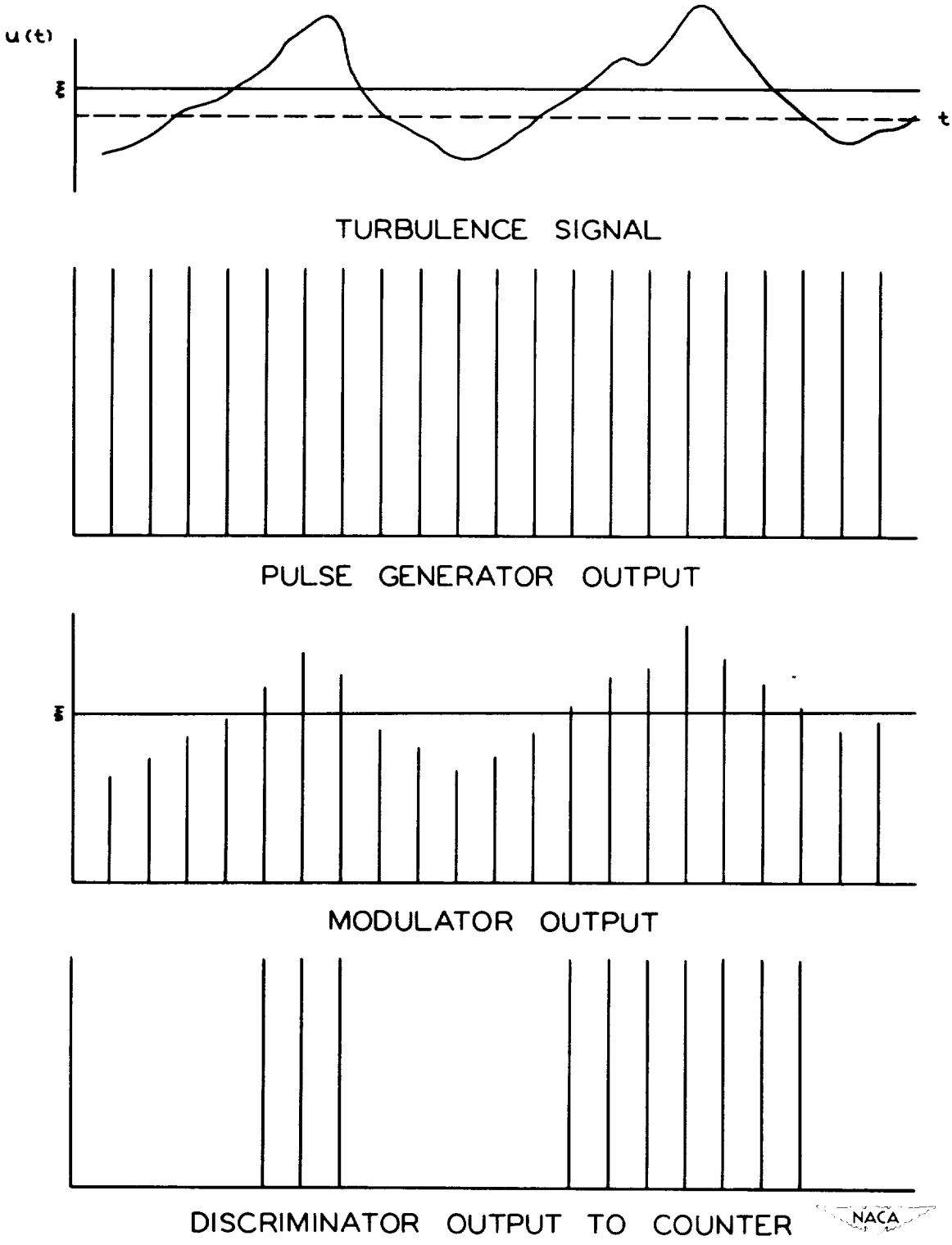

Figure 3.- Representative signal sequence for statistical analyzer.

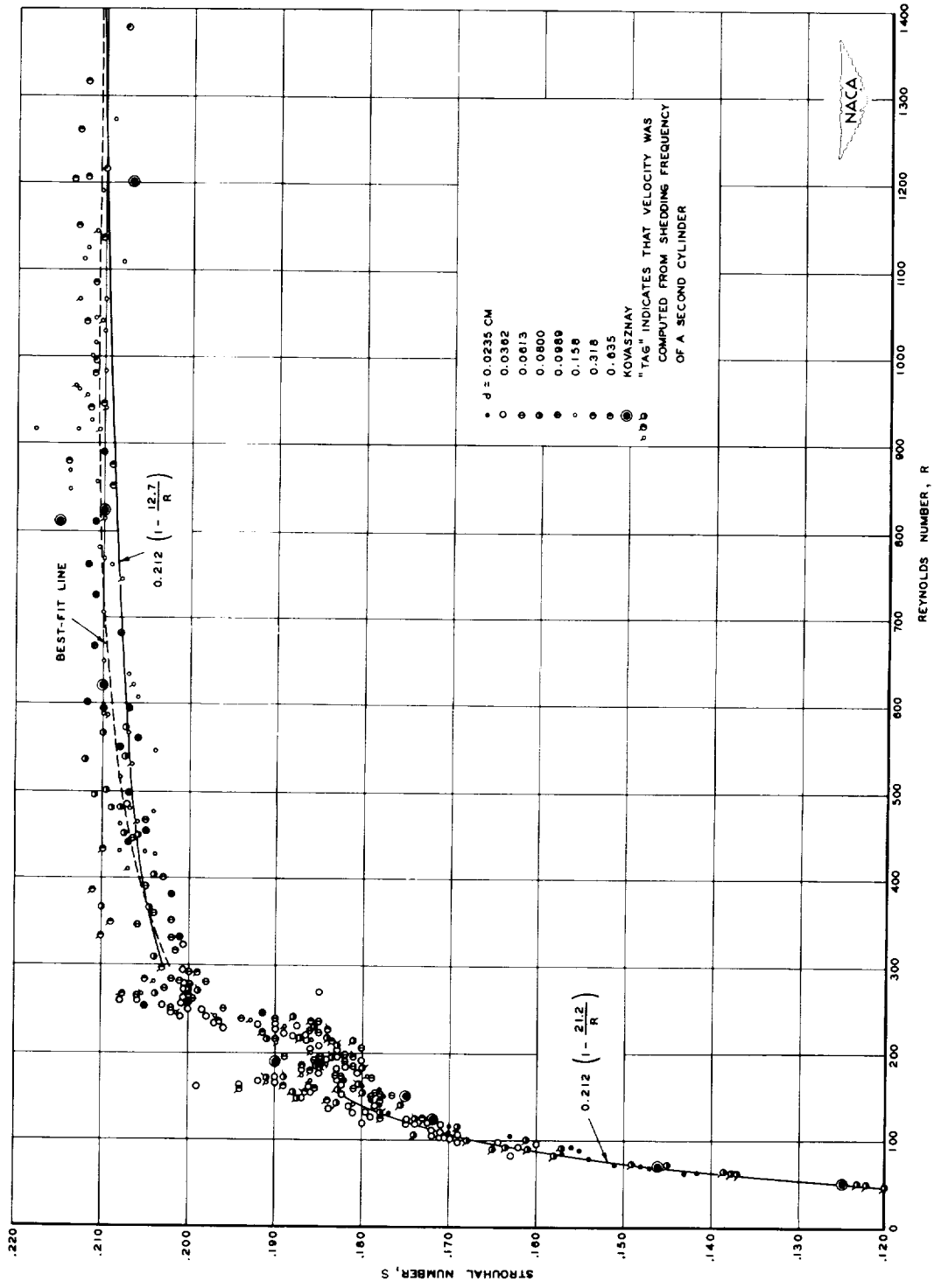

Figure 4.- Strouhal number against Reynolds number for a circular cylinder.

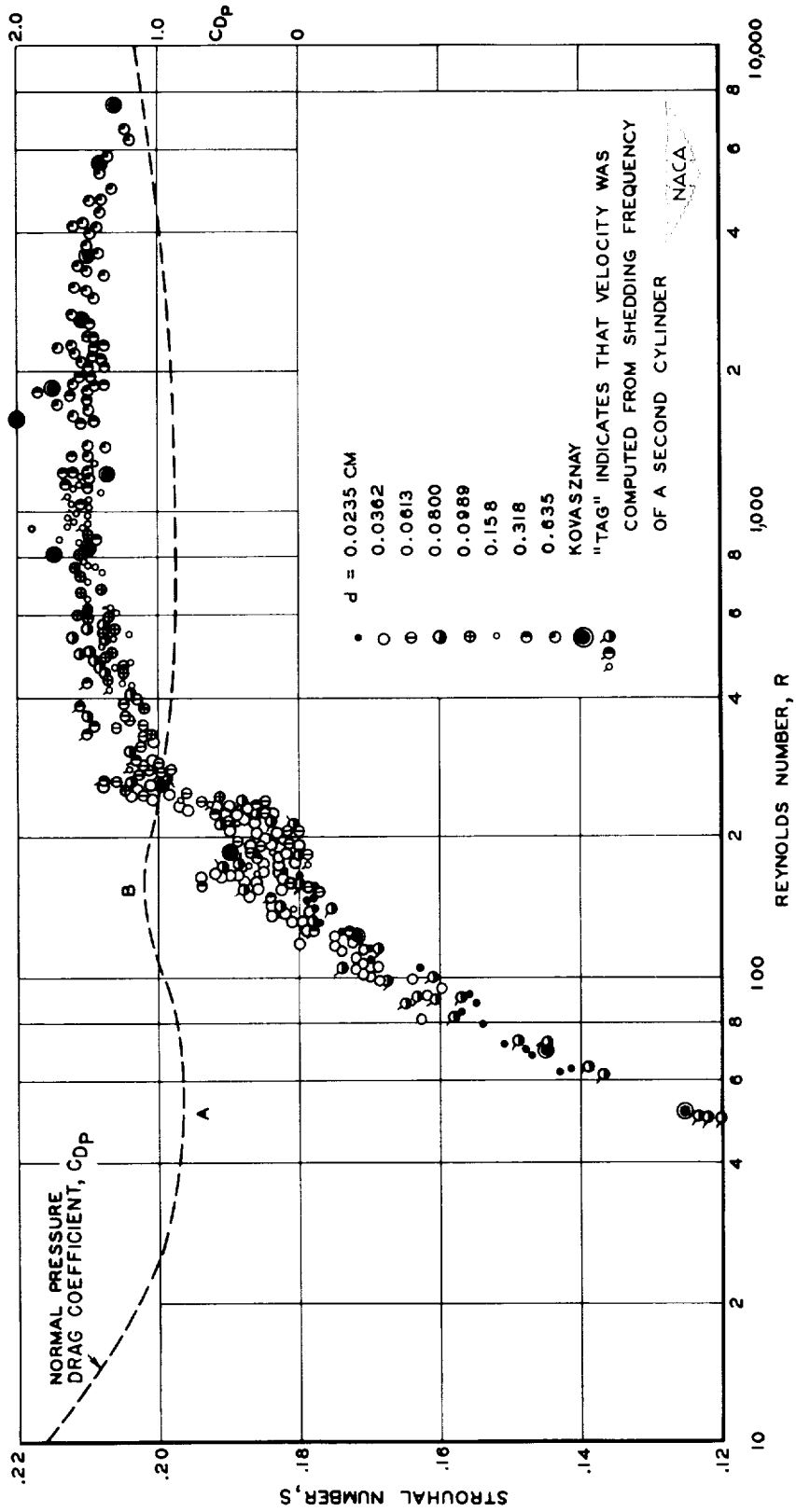

Figure 5.- Strouhal number against Reynolds number for a circular cylinder.

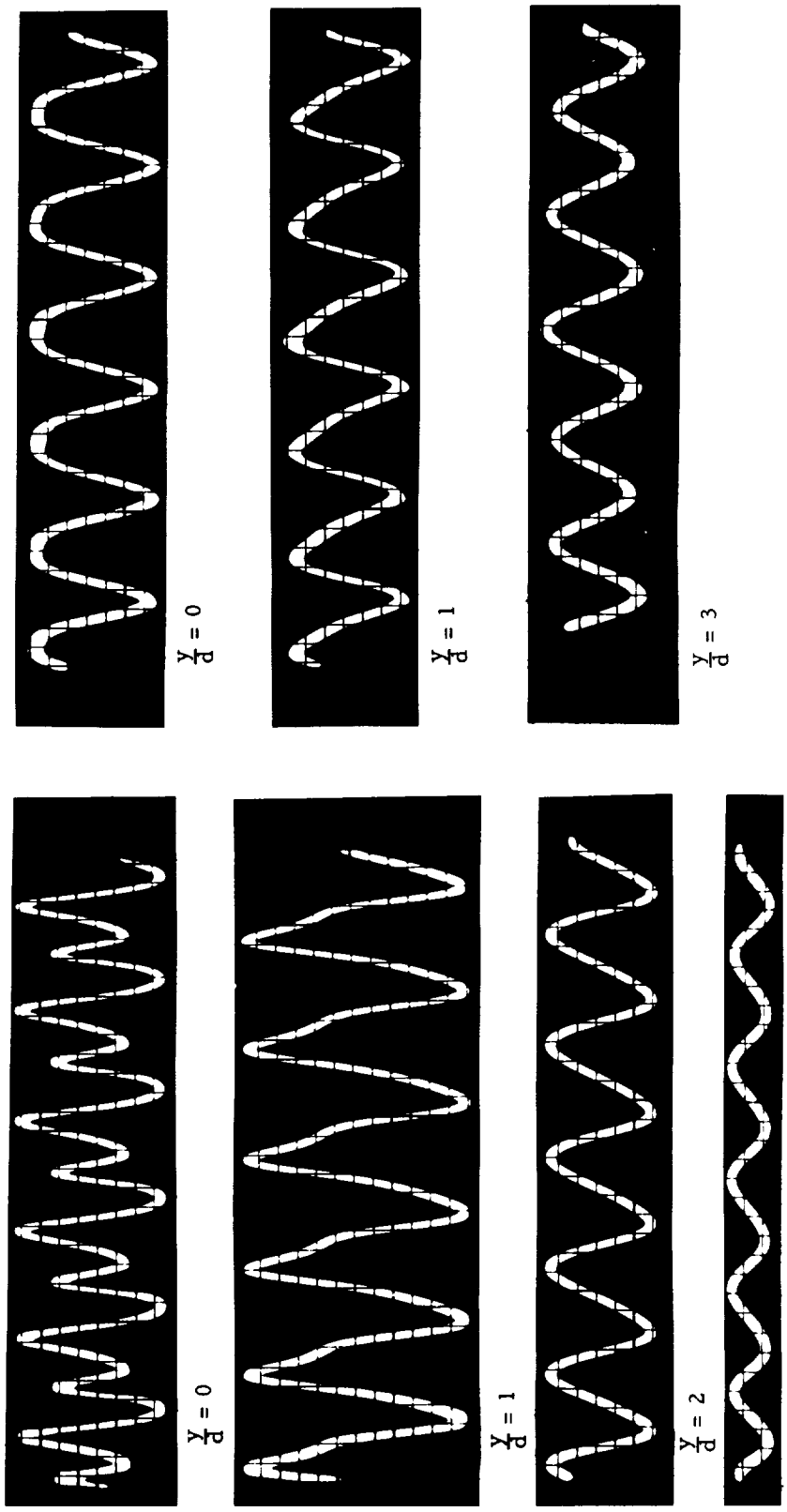

(a) x/d = 6.

(b) x/d = 48.

Figure 6.- Oscillograms for R = 80 and d = 0.158 centimeter.

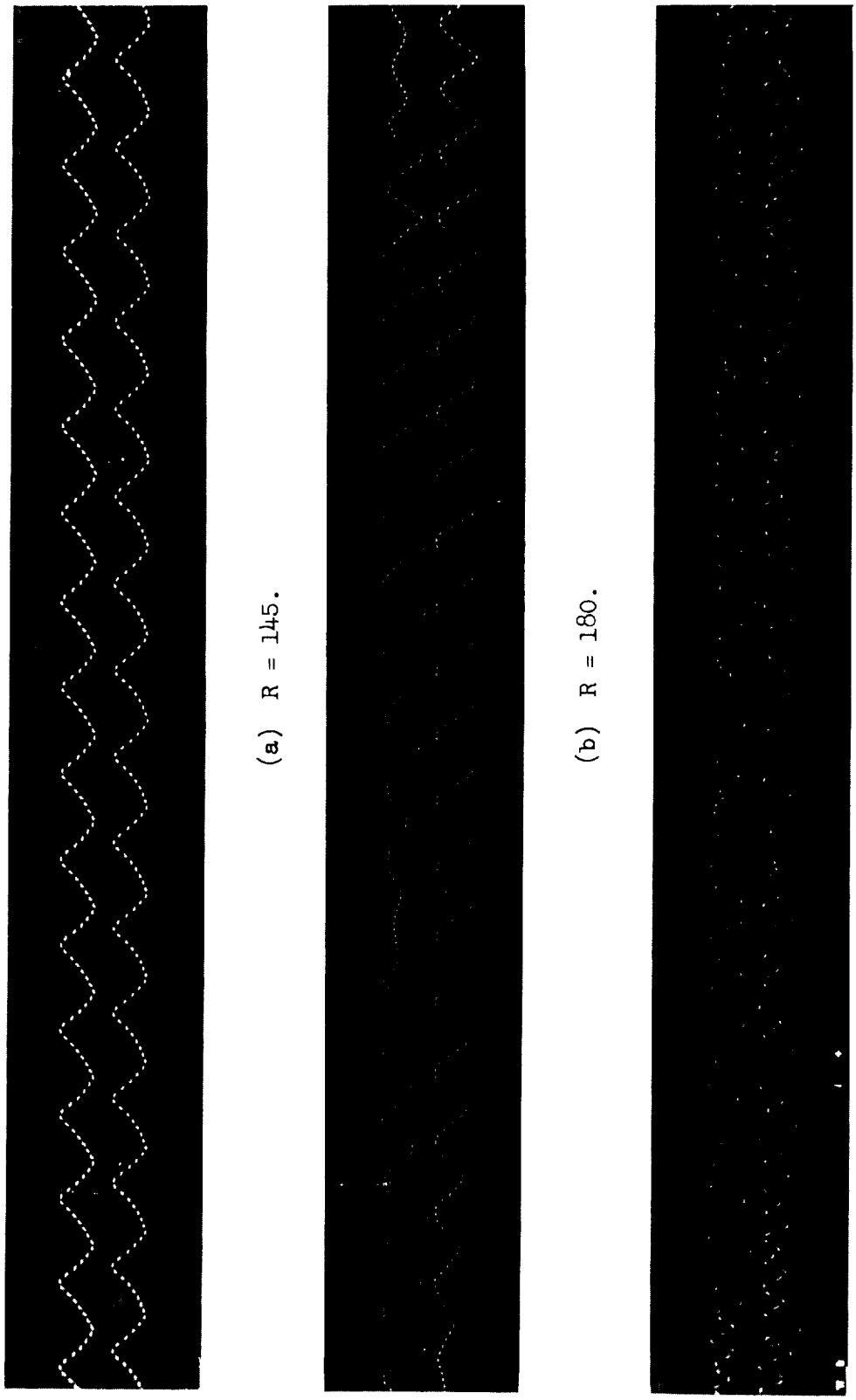

(a) R = 145.

(b) R = 180.

(c) R = 500.

Figure 7.- Simultaneous oscillograms. d = 0.158 centimeter; x/d = 6; y/d = 1; ζ/d = 50.

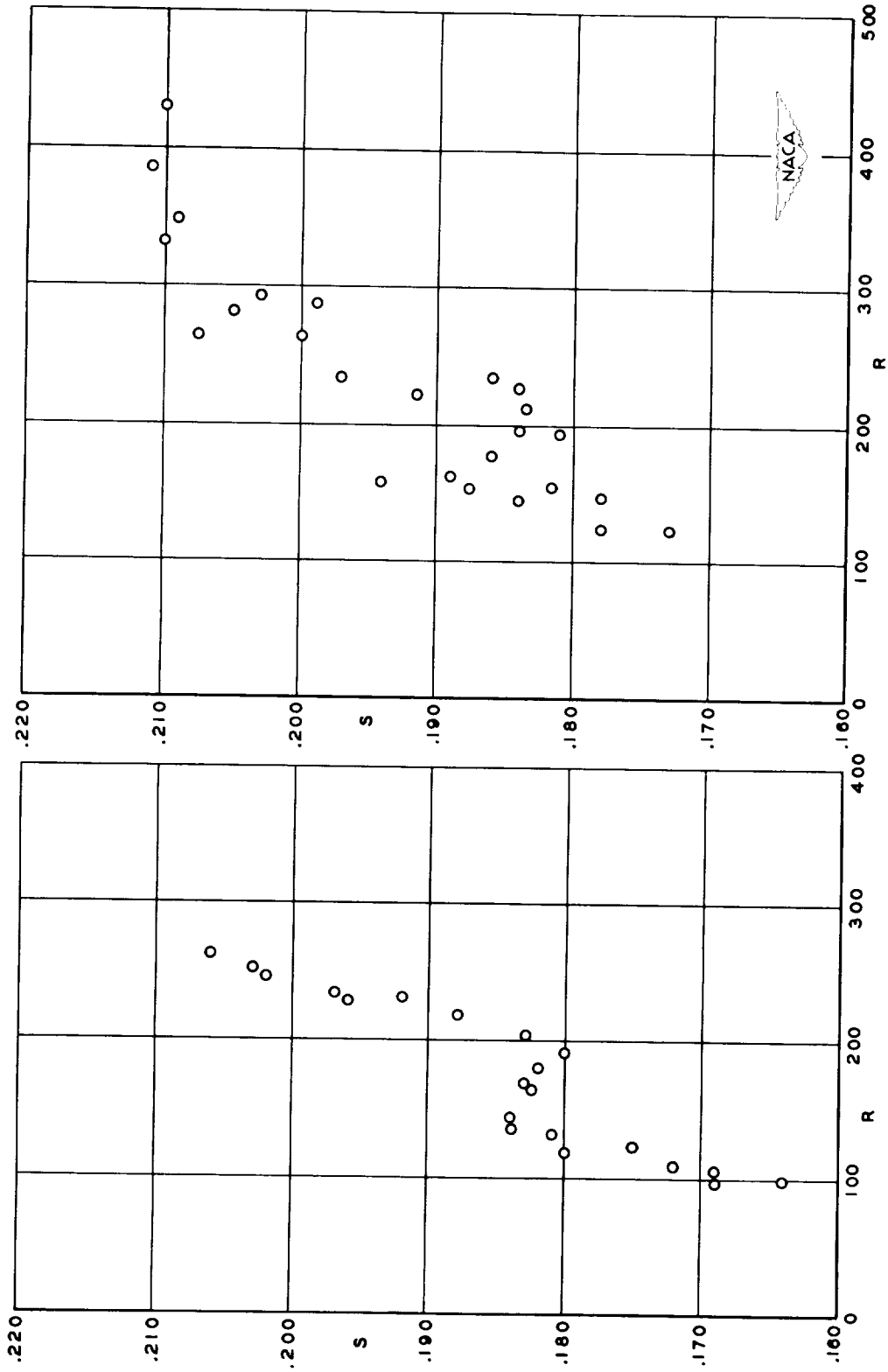

(a) d = 0.0362 centimeter. (b) d = 0.318 centimeter.

Figure 8.- Plot of S(R) for two single runs.

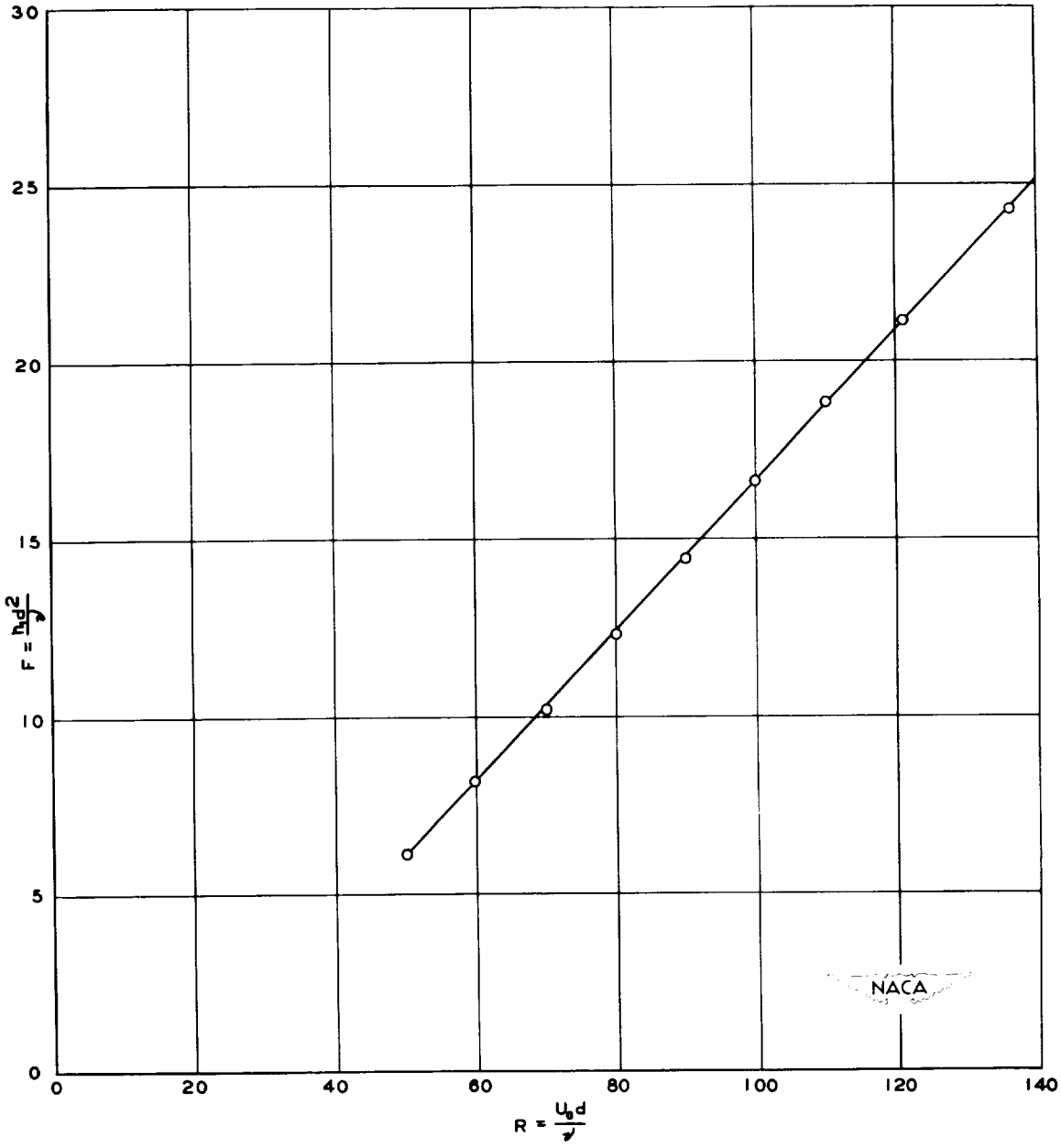

Figure 9.- Plot of F against R ($50 < R < 140$). $F = 0.212R - 4.5$.

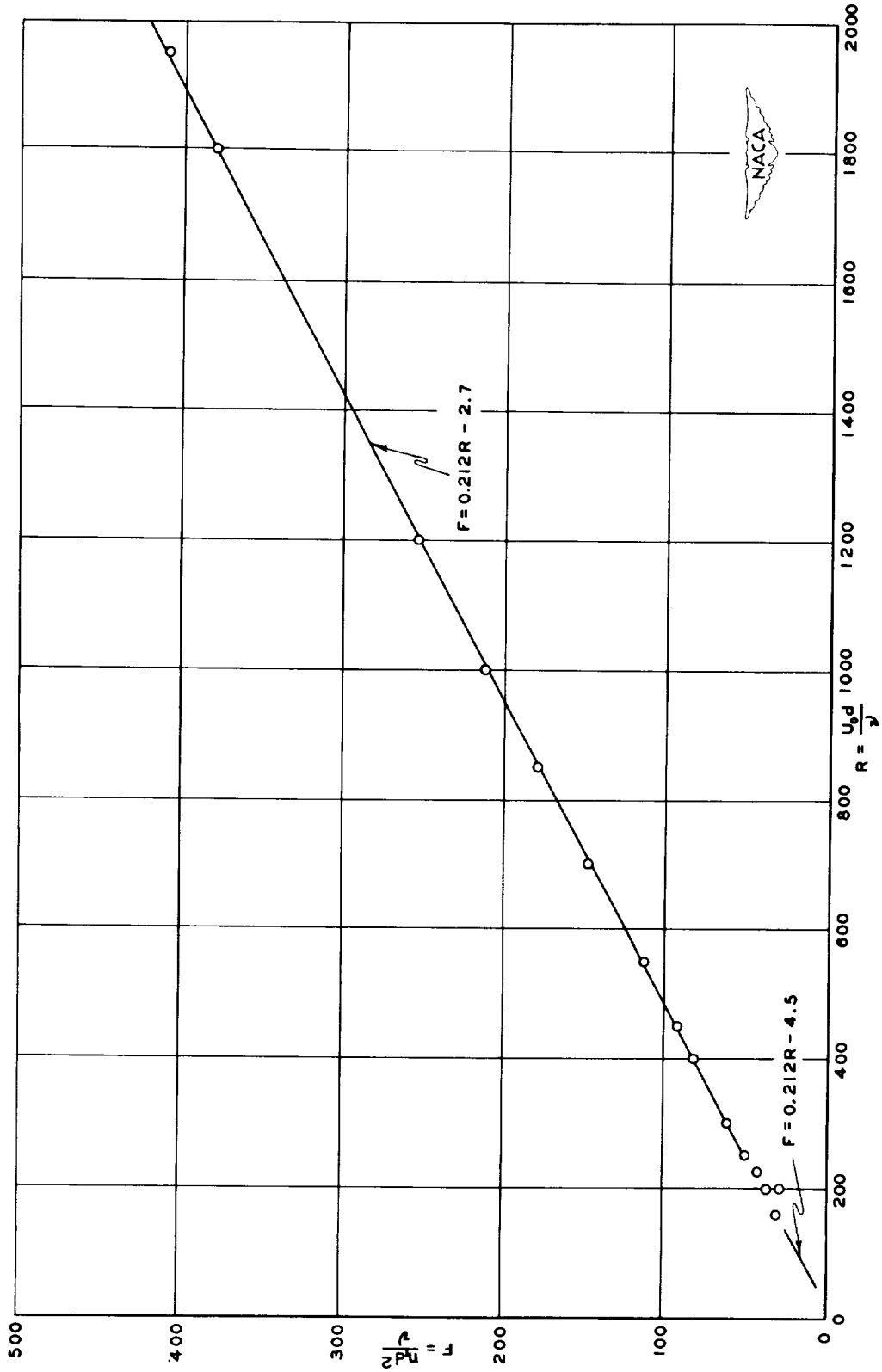

Figure 10.- Plot of F against R $(50 < R < 2000)$.

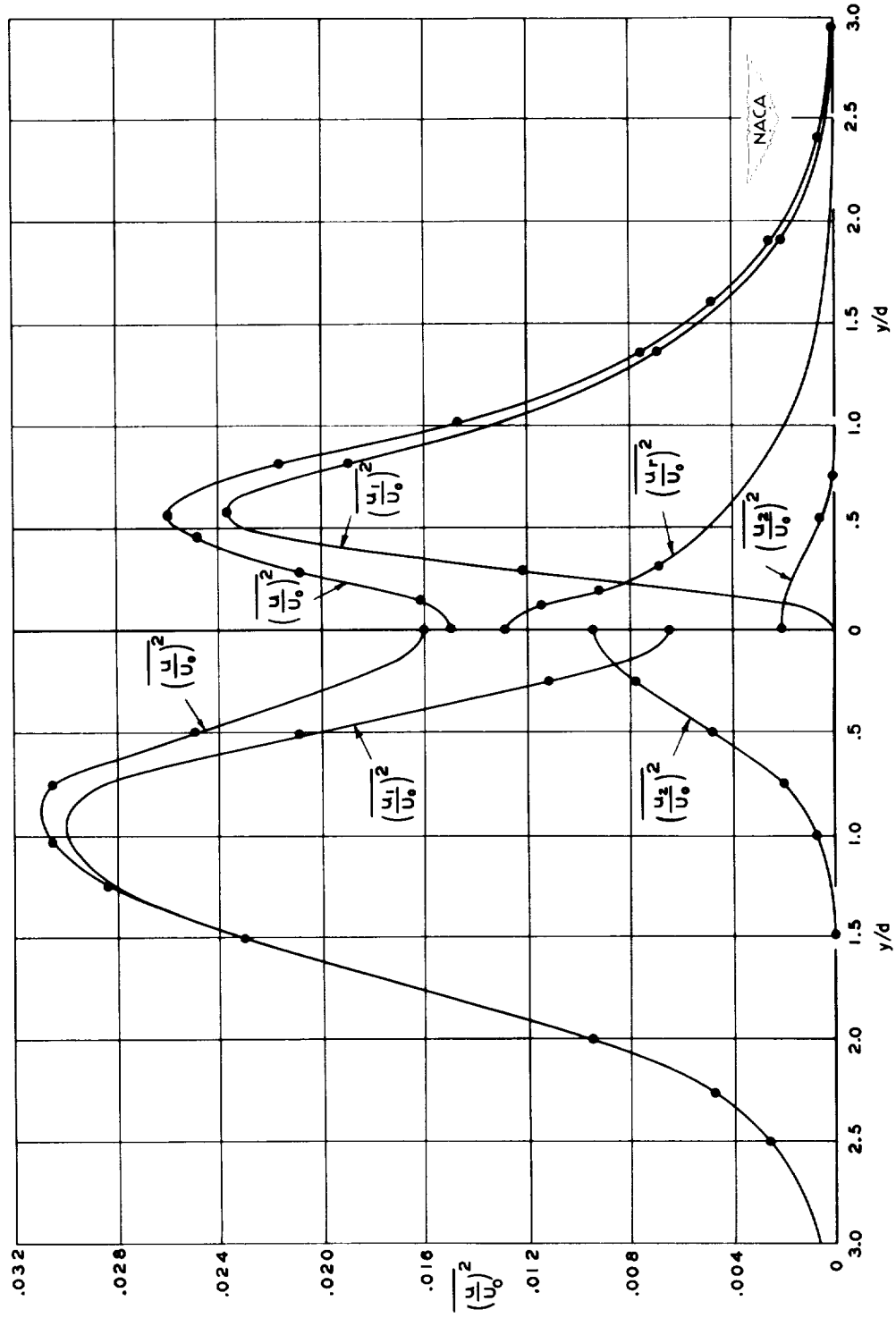

(a) R = 150. (b) R = 500.

Figure 11.- Wake energy. d = 0.190 centimeter; x/d = 6.

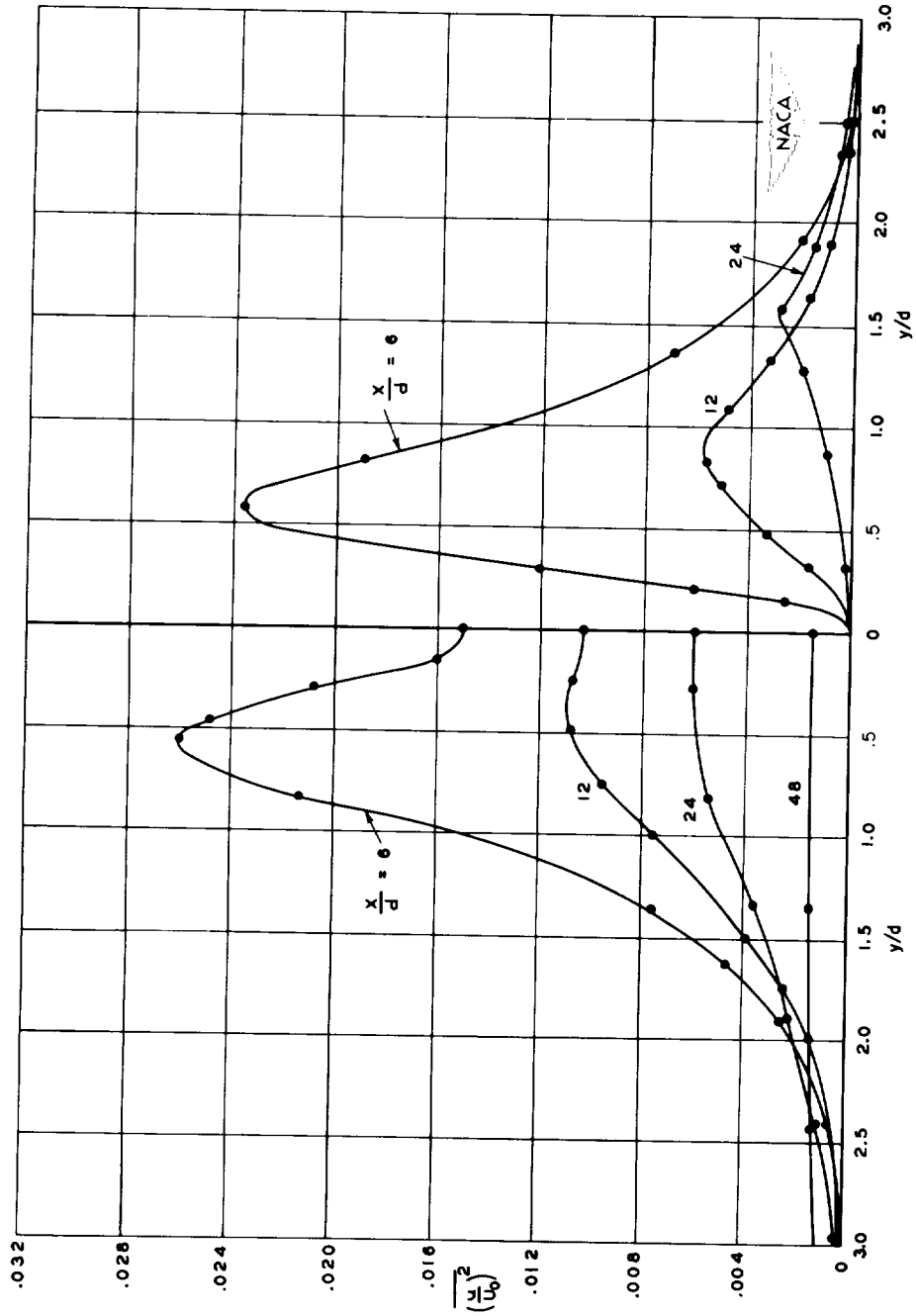

(a) Total energy intensity $\overline{(u/U_o)^2}$.

(b) Discrete energy intensity $\overline{(u_1/U_o)^2}$. Curve for x/d = 24 magnified 10 times for clarity.

Figure 12.- Wake development. d = 0.190 centimeter; R = 500.

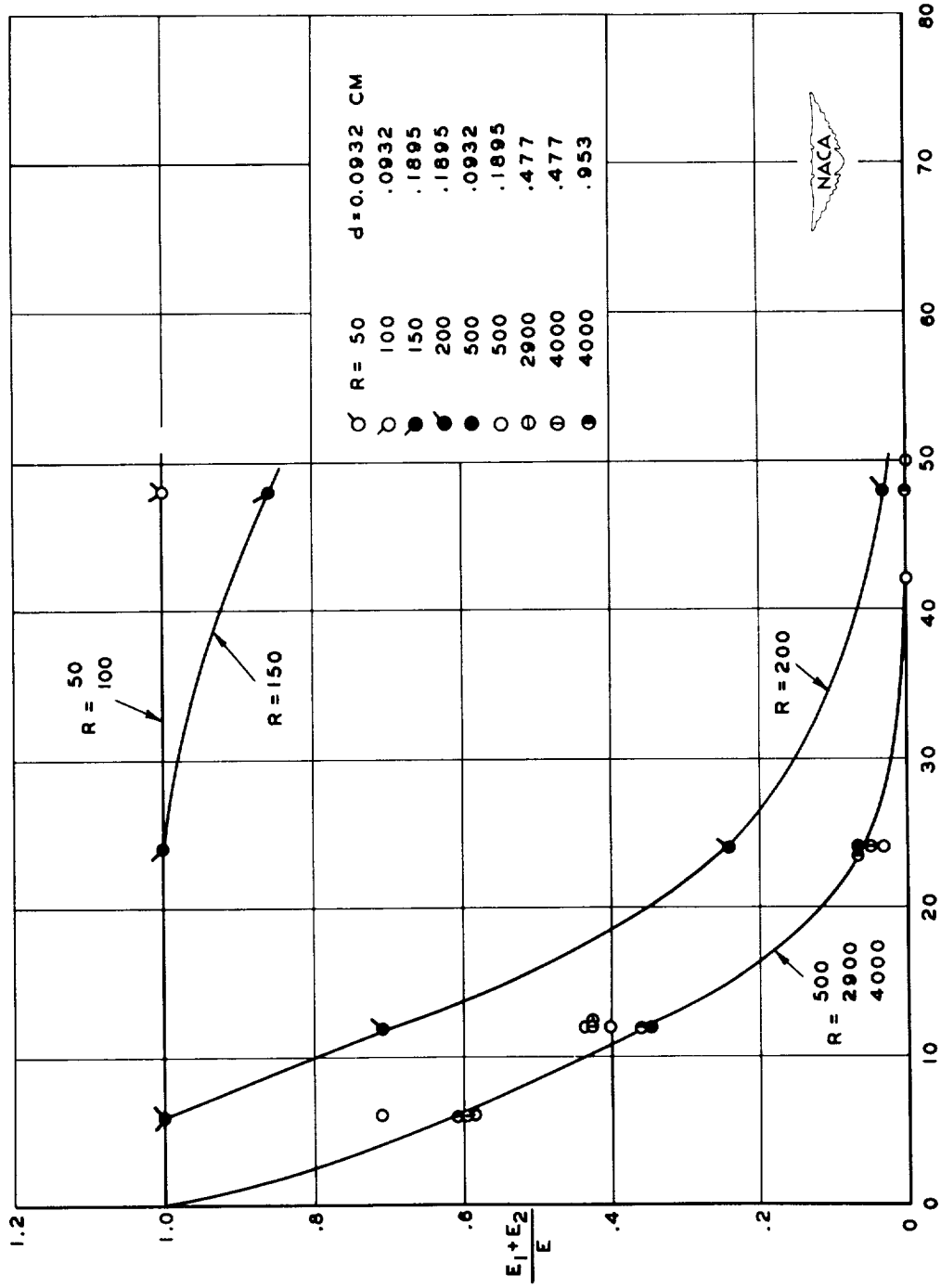

Figure 13.- Decay of discrete energy.

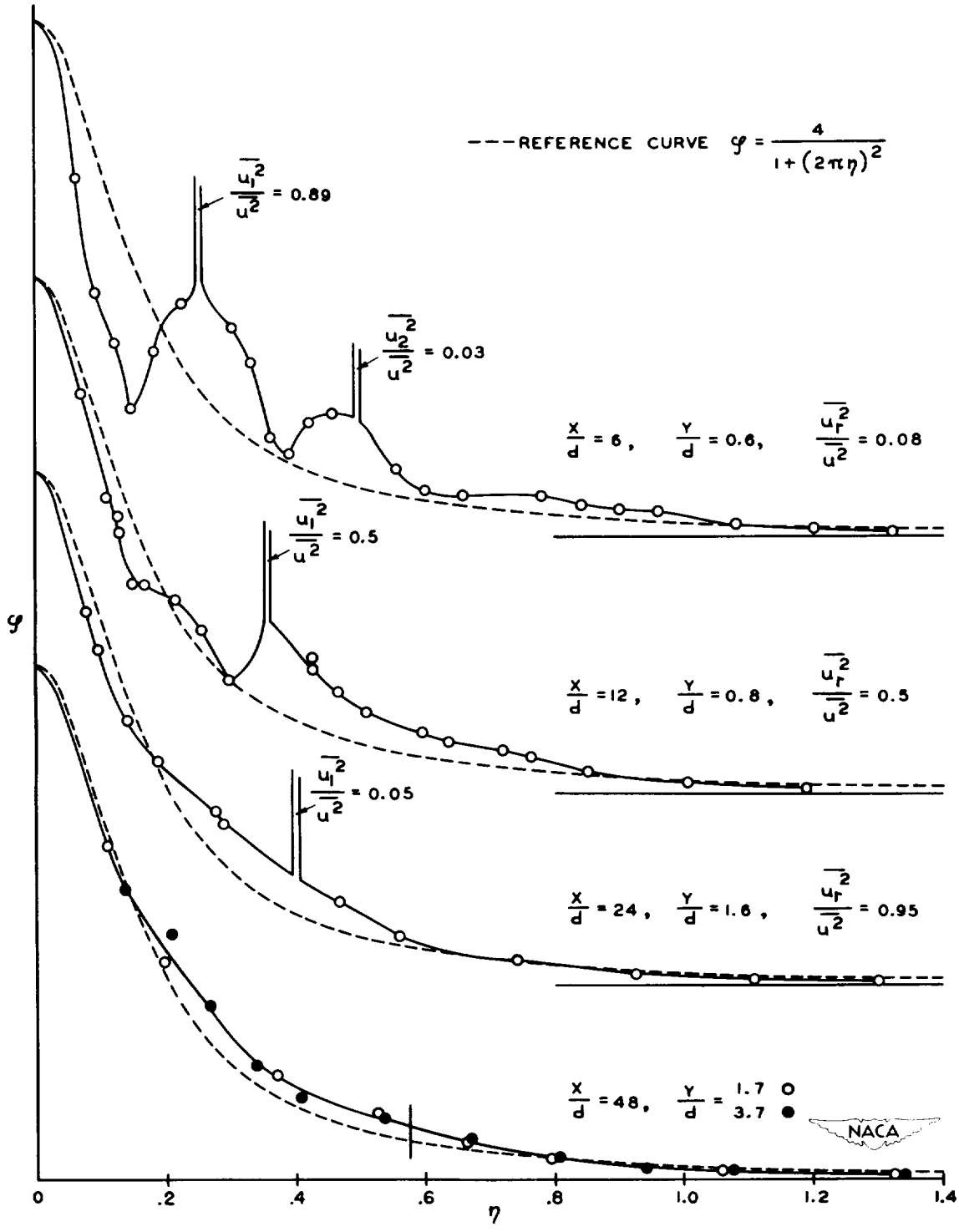

Figure 14.- Downstream development of spectrum. d = 0.190 centimeter; R = 500; n_1 = 440.

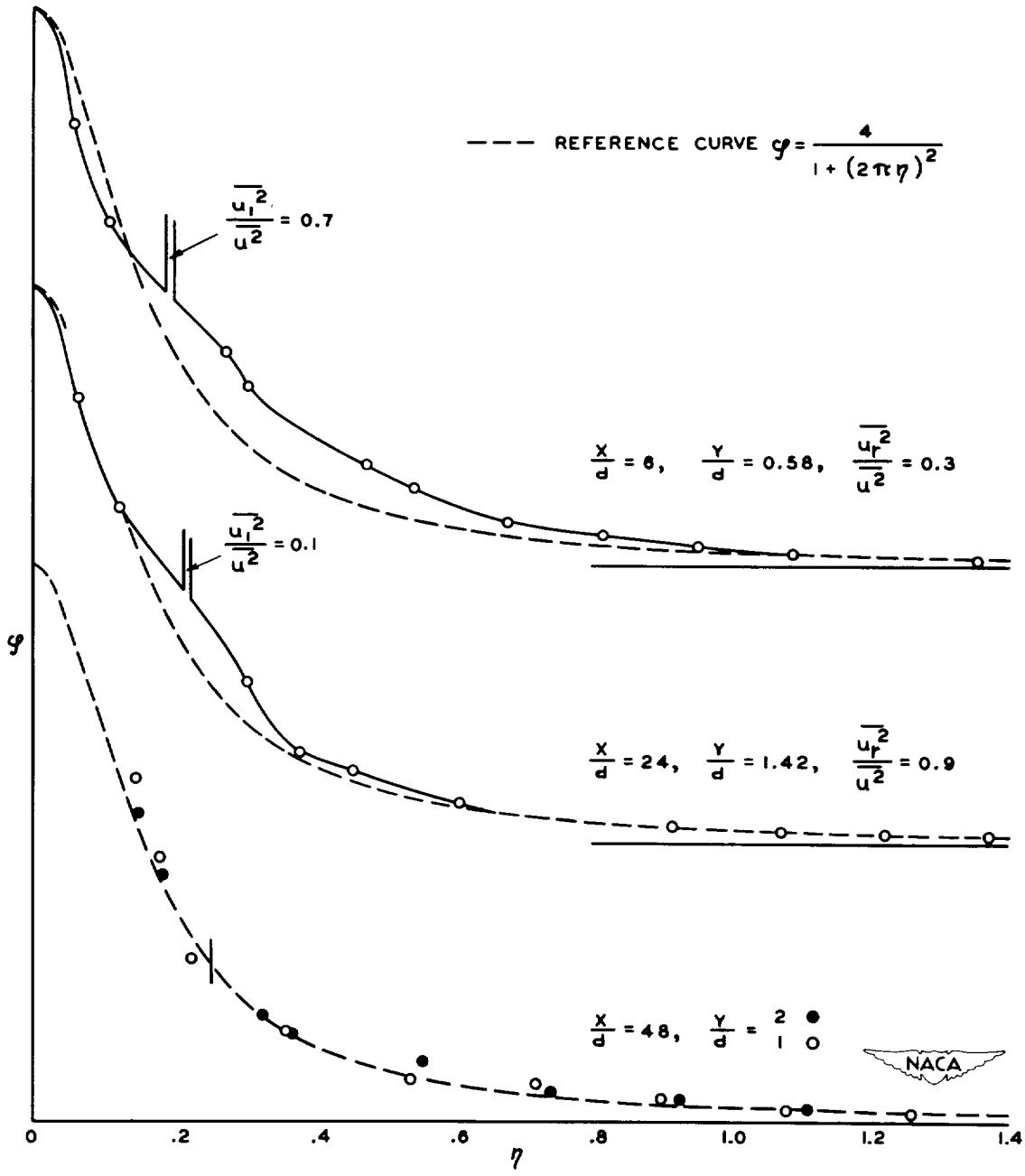

Figure 15.- Downstream development of spectrum. d = 0.953 centimeter; R = 4000; n_1 = 144.

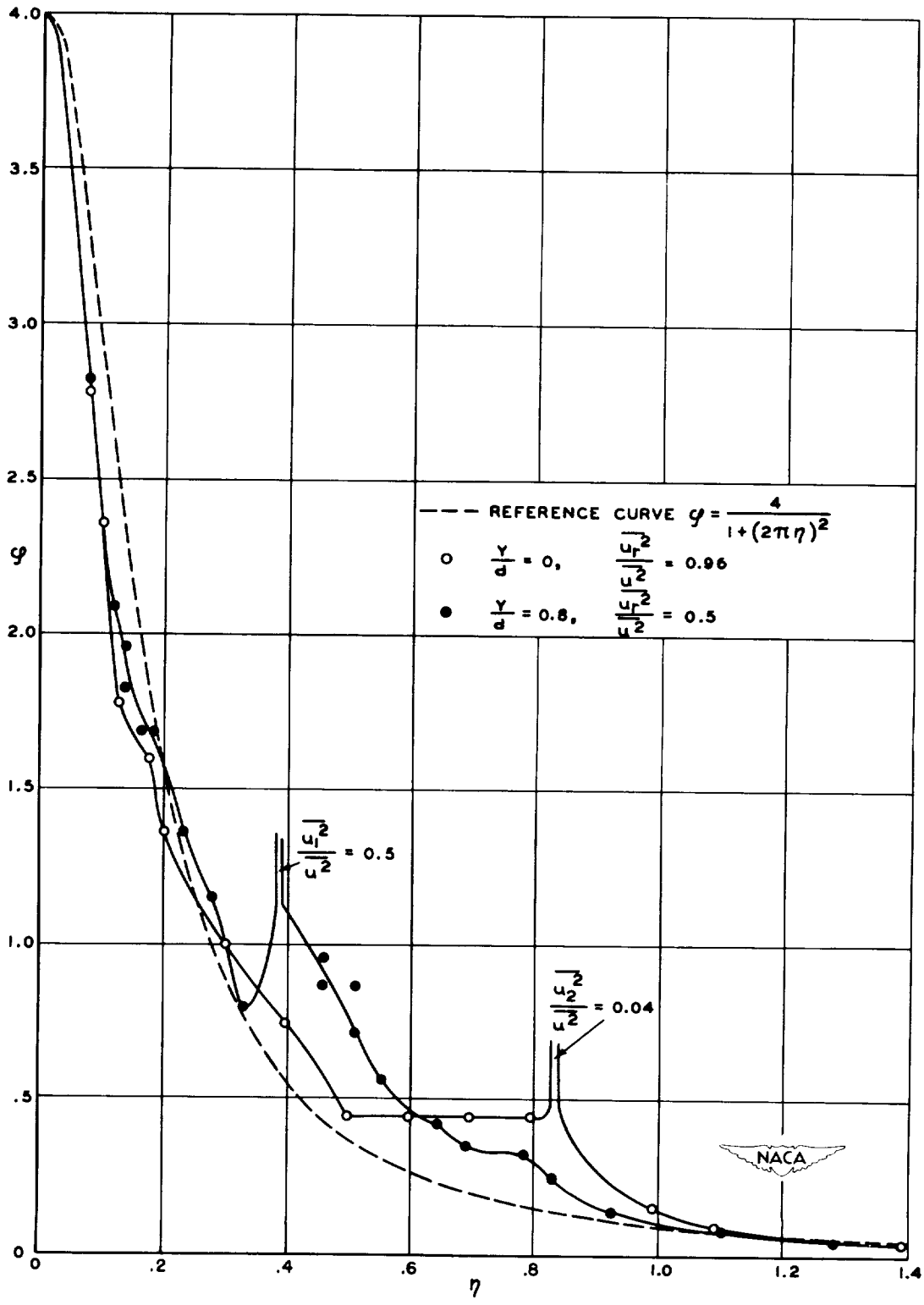

Figure 16.- Spectra at 12 diameters. d = 0.190 centimeter; R = 500; n_1 = 430.

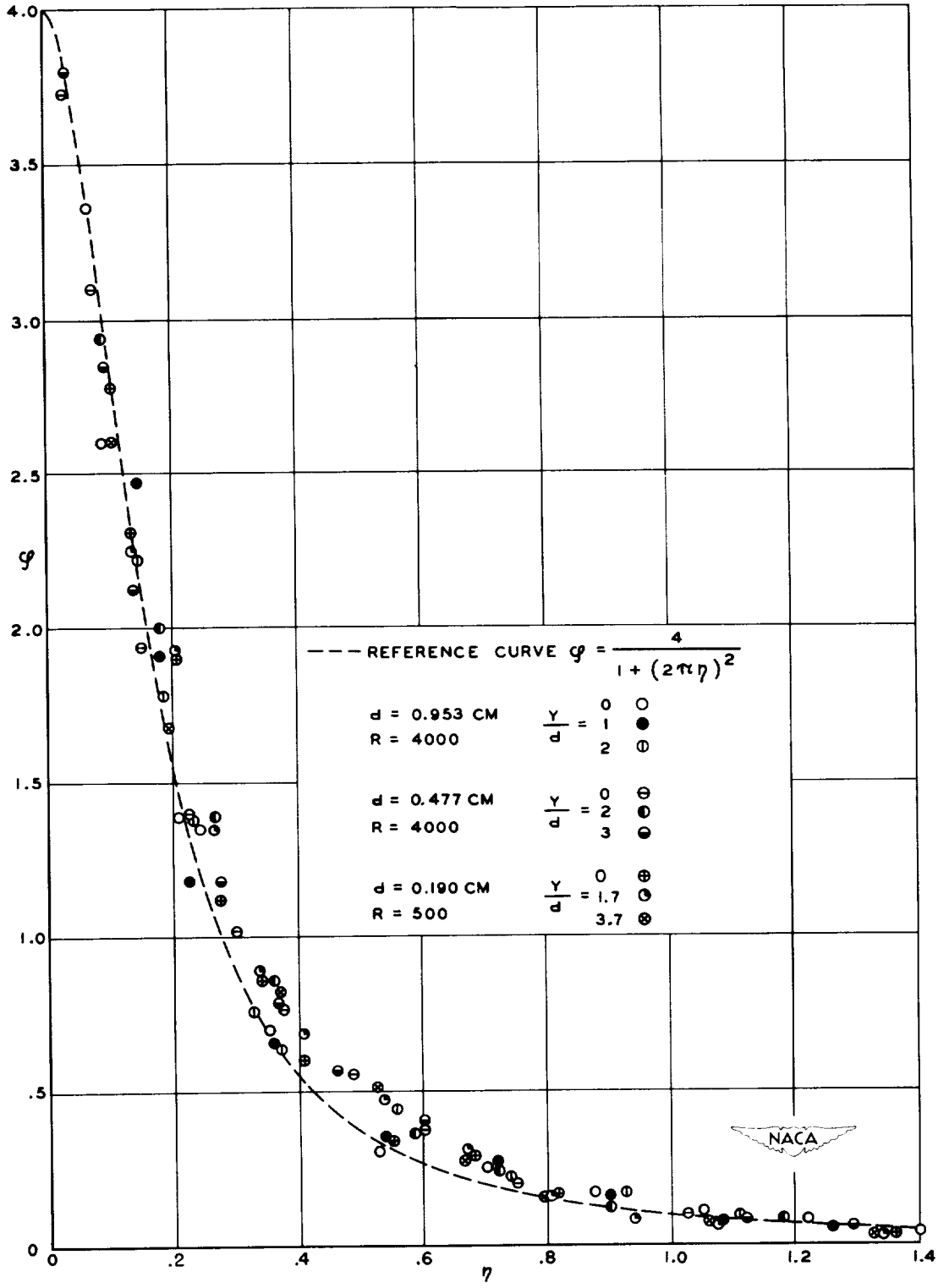

Figure 17.- Spectra at 48 diameters.

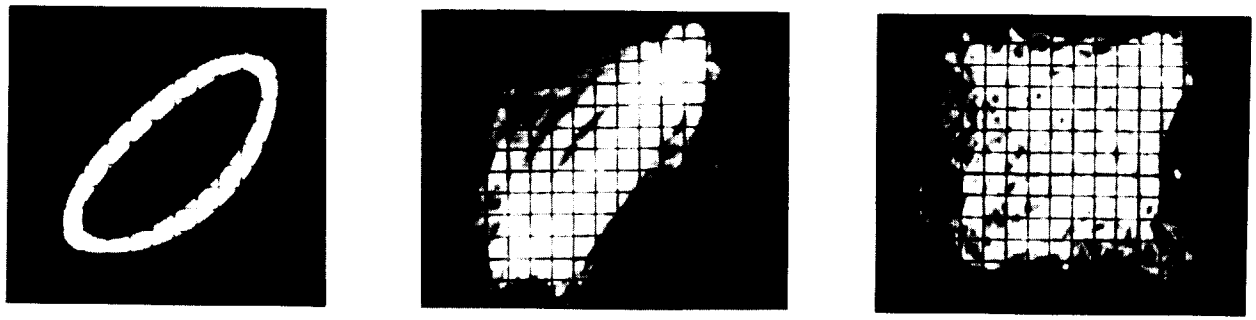

(a) R = 80; ζ/d = 100.

(b) R = 220; ζ/d = 10.

(c) R = 220; ζ/d = 105.

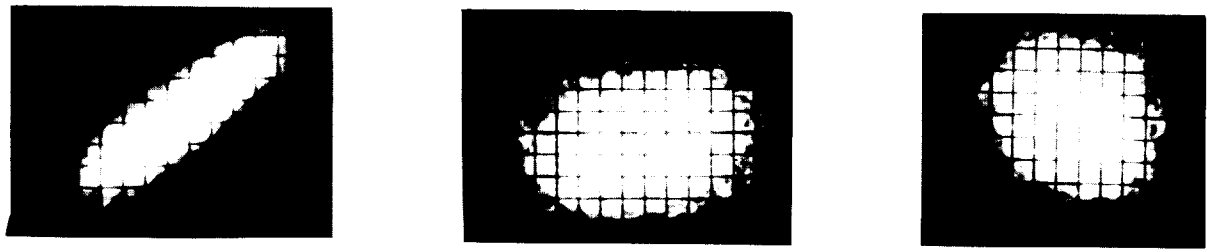

(d) R = 500; ζ/d = 3.

(e) R = 500; ζ/d = 10.

(f) R = 500; ζ/d = 105.

Figure 18.- Correlation figures. d = 0.158 centimeter; x/d = 6; y/d = 1; exposure, $\frac{1}{2}$ second.

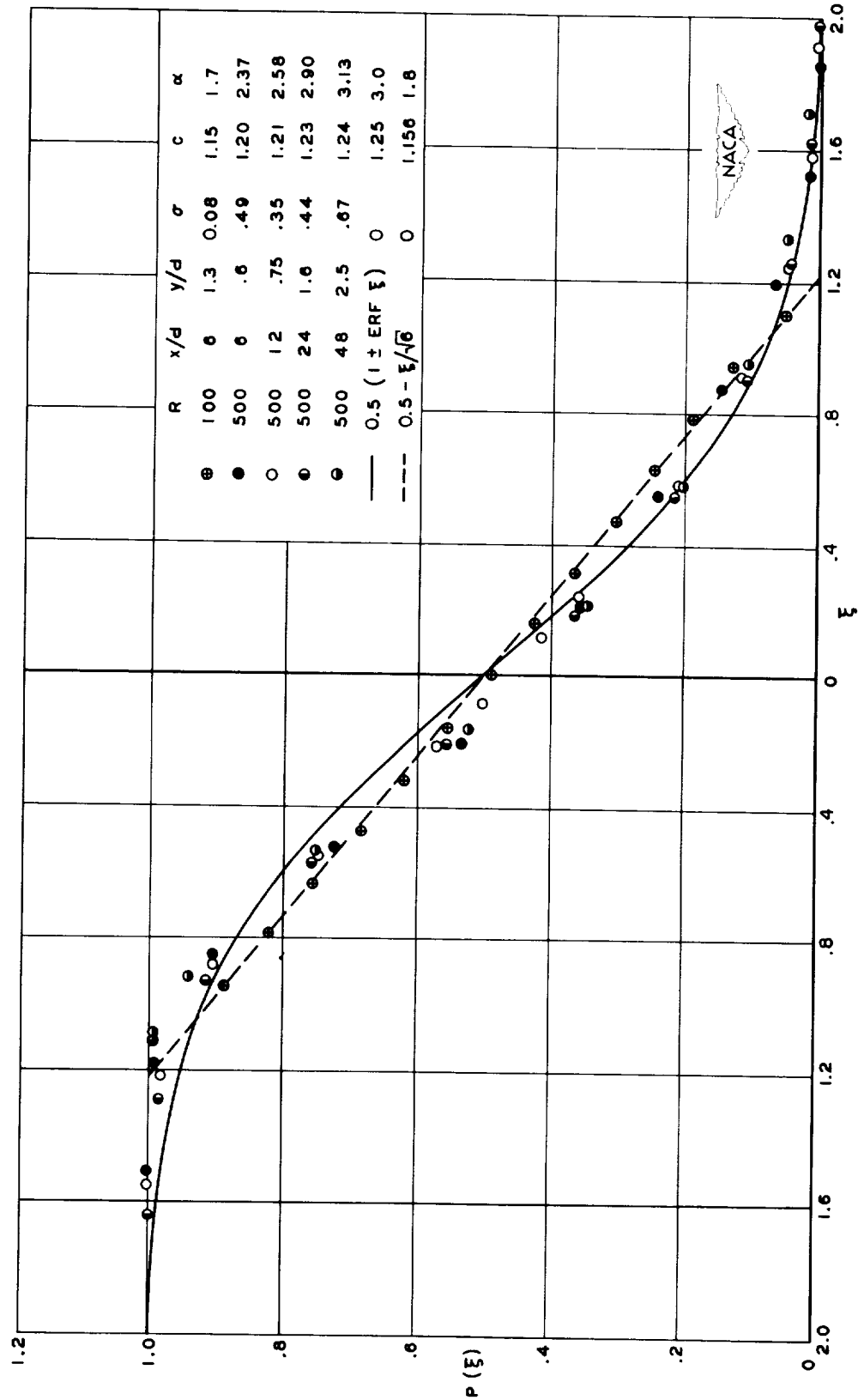

Figure 19.- Distribution functions. d = 0.190 centimeter.

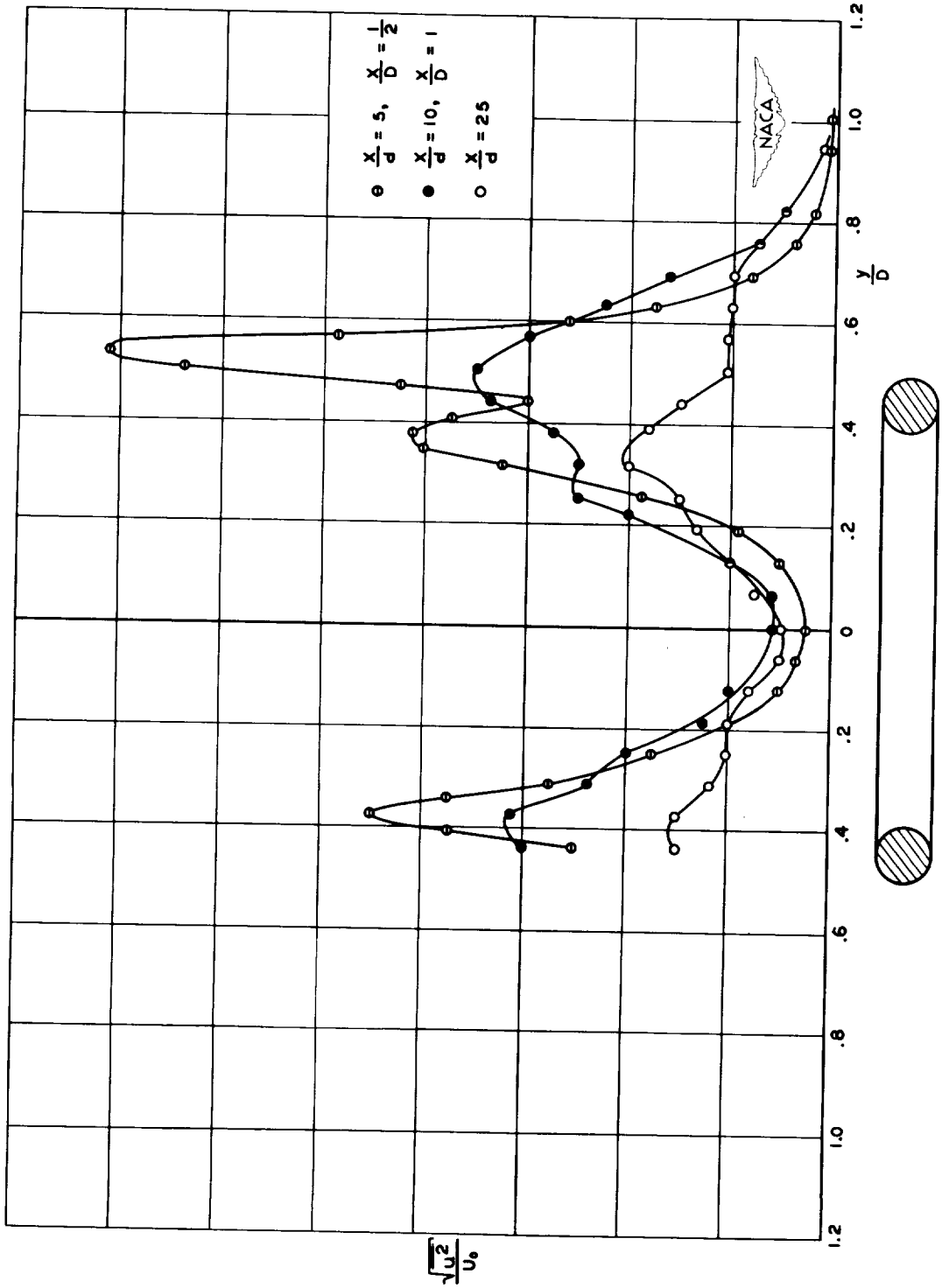

Figure 20.- Shedding from a ring. d = 0.168 centimeter; D = 1.59 centimeters; R = 100; n_1 = 84.

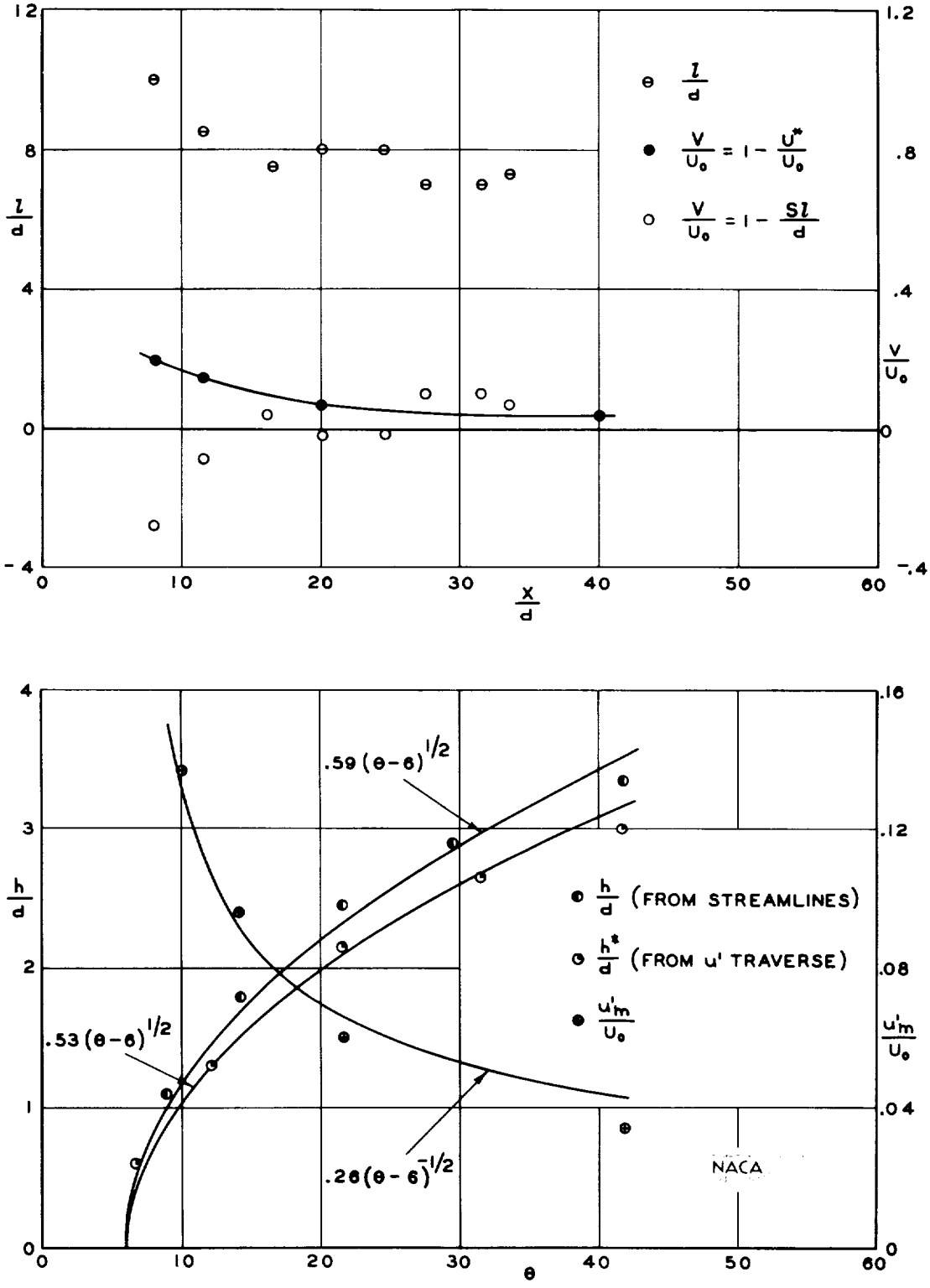

Figure 21.- Vortex-street geometry. Calculated from data in reference 11.

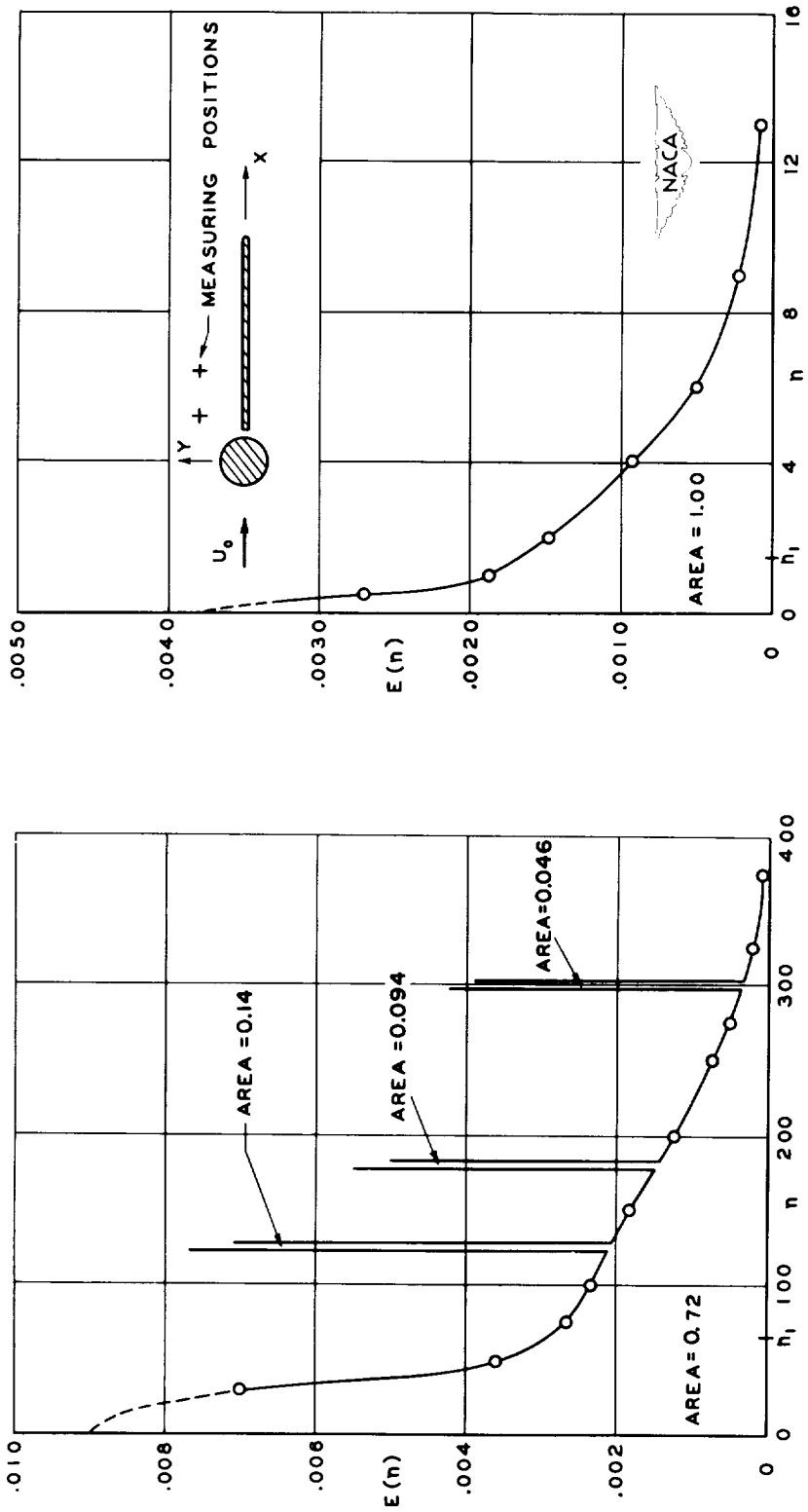

(a) R = 3200; x/d = 2.

(b) R = 7500; x/d = 1.

Figure 22.- Effect of downstream plate on wake frequencies.

NACA-Langley - 3-13-53 - 1000